Atmospheric
Measurement
Techniques

New concepts for the comparison of tropospheric NO₂ column densities derived from car-MAX-DOAS observations, OMI satellite observations and the regional model CHIMERE during two MEGAPOLI campaigns in Paris 2009/10

R. Shaiganfar[1], S. Beirle[1], H. Petetin[2], Q. Zhang[2], M. Beekmann[2], and T. Wagner[1]

[1]Max-Planck-Institute for Chemistry, Mainz, Germany
[2]LISA, UMR CNRS 7583, Université Paris Est Créteil et Université Paris Diderot, Institut Pierre Simon Laplace, Créteil, France

Correspondence to: R. Shaiganfar (r.shaiganfar@mpic.de)

Abstract. We compare tropospheric column densities (vertically integrated concentrations) of NO₂ from three data sets for the metropolitan area of Paris during two extensive measurement campaigns (25 days in summer 2009 and 29 days in winter 2010) within the European research project MEGAPOLI. The selected data sets comprise a regional chemical transport model (CHIMERE) as well as two observational data sets: ground-based mobile Multi-AXis-Differential Optical Absorption Spectroscopy (car-MAX-DOAS) measurements and satellite measurements from the Ozone Monitoring Instrument (OMI). On most days, car-MAX-DOAS measurements were carried out along large circles (diameter ∼ 35 km) around Paris. The car-MAX-DOAS results are compared to coincident data from CHIMERE and OMI. All three data sets have their specific strengths and weaknesses, especially with respect to their spatiotemporal resolution and coverage as well as their uncertainties. Thus we compare them in two different ways: first, we simply consider the original data sets. Second, we compare modified versions making synergistic use of the complementary information from different data sets. For example, profile information from the regional model is used to improve the satellite data, observations of the horizontal trace gas distribution are used to adjust the respective spatial patterns of the model simulations, or the model is used as a transfer tool to bridge the spatial scales between car-MAX-DOAS and satellite observations. Using the modified versions of the data sets, the comparison results substantially improve com-

pared to the original versions. In general, good agreement between the data sets is found outside the emission plume, but inside the emission plumes the tropospheric NO₂ vertical column densities (VCDs). are systematically underestimated by the CHIMERE model and the satellite observations (compared to the car-MAX-DOAS observations). One major result from our study is that for satellite validation close to strong emission sources (like power plants or megacities), detailed information about the intra-pixel heterogeneity is essential. Such information may be gained from simultaneous car-MAX-DOAS measurements using multiple instruments or by combining (car-) MAX-DOAS measurements with results from regional model simulations.

1 Introduction

Nitrogen oxides (NO$_x$ = NO + NO₂) play an important role in tropospheric chemistry as they impact oxidising capacity and ozone formation (Atkinson, 2000; Seinfeld and Pandis, 2012). NO$_x$ emissions are dominated by anthropogenic activities, e.g. from traffic and power generation. Emissions from megacities have a strong influence on the regional and global air quality; thus accurate estimates of megacity emissions are highly required. For instance, urban NO₂ concentrations in Paris still represent an important air quality problem (Airparif, 2014), with the European annual limit value of

40 µg m^{-3} being exceeded not only at the urban traffic sites, but also frequently at urban background sites. This calls for further studies including evaluation of urban emissions. One possibility to quantify NO$_x$ emissions from megacities is to use so-called "top-down approaches" based on remote sensing observations, e.g. from satellite (Leue et al., 2001; Martin et al., 2003; Beirle et al., 2011) or ground-based observations (Rivera et al., 2009; Ibrahim et al., 2010; Shaiganfar et al., 2011). Usually top-down emission estimates require inverse modelling or estimates of the atmospheric lifetimes of the considered species. Accordingly, major uncertainties of top-down emission estimates are related to (i) the uncertainties of the remote sensing measurements and (ii) the ability of the models to accurately simulate atmospheric chemistry and physics.

NO$_2$, which typically constitutes the major fraction of NO$_x$ (Seinfeld and Pandis, 2012), can be measured by remote sensing techniques in the visible spectral range (e.g. Brewer et al., 1973; Noxon, 1975; Roscoe et al., 1999). For the estimation of NO$_x$ emissions, usually two types of remote sensing measurements: (i) satellite observations (e.g. Leue et al., 2001; Richter and Burrows, 2002; Martin et al., 2002; Beirle et al., 2003; Boersma et al., 2004; Richter et al., 2005) from the Ozone Monitoring Instrument (OMI) (Levelt et al., 2006), and (ii) so-called Multi-AXis- (MAX-) DOAS observations (e.g. Hönninger and Platt, 2002; Van Roozendael et al., 2004; Wittrock et al., 2004; Brinksma et al., 2008; Wagner et al., 2011) are used.

In this study, we present car-MAX-DOAS observations of tropospheric NO$_2$ along variable driving routes around Paris during the MEGAOPLI campaign. The work presented in this paper investigates the consistency of the car-MAX-DOAS observations with satellite measurements from OMI. In addition to these experimental data sets, results from a regional chemistry transport model (CTM) CHIMERE (see e.g. Schmidt et al., 2001; Menut et al., 2013) are included in the comparison. In a forthcoming second paper, NOx emissions from Paris are estimated from the car-MAX-DOAS observations made in circles around Paris, and the resulting emissions are compared to emission inventories (compare e.g. Ibrahim et al., 2010; Wagner et al., 2010; Shaiganfar et al., 2011).

Here it should be noted that since 2005, ground-based observations are performed in Paris using a zenith sky instrument (Dieudonné et al., 2013). From these measurements important information on the seasonal/diurnal cycle of NO$_2$ could be derived. In addition, Dieudonné et al. (2013) could show that the NO$_2$ concentrations systematically decrease with increasing altitude. Modelling with the CHIMERE model of the surface NO$_x$ measurements at three urban and suburban sites during the MEGAPOLI summer campaign (July 2009) showed a reasonable correlation (0.55–0.65), but a significant overestimation between 22 and 95 % (Zhang et al., 2013). Vertically integrated NO$_2$ column measurements could help to distinguish, if such a bias is due to emissions

or to errors in vertical mixing. Deguillaume et al. (2007) used urban NO and O$_3$ concentrations from the AirParif network to constrain urban and plume ozone concentrations in a Bayesian Monte Carlo framework. For summers 1998 and 1999, they found good agreement between urban background NO concentrations (12.8 ppb, average over 5 sites) and simulations with the CHIMERE model (12.6 ppb).

Compared to previous car-MAX-DOAS measurements around emission sources (e.g. Rivera et al., 2009; Ibrahim et al., 2010; Shaiganfar et al., 2011), our study is special in many respects.

a. Our car-MAX-DOAS measurements cover many days in two seasons (summer 2009 and winter 2009/2010). Thus with respect to spatial and temporal coverage our comparison between car-MAX-DOAS and satellite observations goes beyond most existing comparisons (e.g. Brinksma et al., 2008; Chen et al., 2009; Hains et al., 2010; Shaiganfar et al., 2011; Irie et al., 2012; Ma et al., 2013; Lin et al., 2014).

b. We systematically compare our measurements with simultaneous satellite and model data sets.

c. We make synergistic use of the different data sets by combination their specific advantages. Thus the specific uncertainties of all used data sets are minimised. The regional model is used as a transfer tool to correct for the differences in spatial resolution.

The paper is organised in the following way: in Sects. 2 and 3 we describe the data sets, their specific advantages and limitations and how to use them in a synergistic way. In Sects. 4 and 5 CHIMERE model data are compared to car-MAX-DOAS and OMI observations, respectively. Section 6 presents the comparison of coincident observations of all three data sets. A summary and outlook are provided in Sect. 7.

2 Data sets

The car-MAX-DOAS observations in and around Paris were performed during two extensive measurement campaigns organised in the frame of the MEGAPOLI project (Mahura and Baklanov, 2012; see also http://megapoli.dmi.dk/). In June and July 2009 car-MAX-DOAS measurements were performed on 25 days, and in January and February 2010 on 29 days. For almost all of these days model results from CHIMERE are available. OMI satellite observations are also available for most days, although many of these observations provide only limited information on the tropospheric NO$_2$ abundance due to the presence of clouds. The three data sets are described in the following sub-sections.

2.1 Car-MAX-DOAS

Car-MAX-DOAS observations were performed by a temperature-stabilised mini-MAX-DOAS instrument which is described in detail in Wagner et al. (2010), Ibrahim et al. (2010) and Shaiganfar et al. (2011). Here a brief overview is given. The MAX-DOAS instrument is mounted on top of a car in backward direction. The telescope (field of view $\sim 1.2°$) is directed to different elevation angles with integration times of 1 min. The following sequence of elevation angles was chosen: $90°$, $5 \times 22°$, $45°$, $5 \times 22°$ (the measurement sequence is repeated after 12 individual measurements). This choice optimises the number of measurements at low elevation angles, from which we derive the tropospheric vertical column density (VCD). The measurements at elevation angles of $45°$ and $90°$ are used for the determination of the NO$_2$ absorption in the Fraunhofer reference spectrum and are needed at lower frequency (Wagner et al., 2010). For typical driving speeds, this corresponds to a spatial resolution of ~ 1 km. The spectral range of the instrument is 320–460 nm with a spectral resolution of ~ 0.7 nm (full width at half maximum).

The first step of the data analysis comprises the spectral analysis using the DOAS technique (Platt and Stutz, 2008). The spectral range from 420 to 460 nm was used, and in addition to the NO$_2$ cross section (294 K, Vandaele et al., 1997) also those of H$_2$O (290 K, Rothman et al., 2005), CHOCHO (Volkamer et al., 2005), O$_3$ (343 K, Bogumil et al., 2003), and O$_4$ (296 K, Hermans et al., 1999) and a synthetic Ring spectrum (Wagner et al., 2009) were included. A daily measurement in zenith direction is used as so-called Fraunhofer reference spectrum. Measurements for which the light path was blocked by trees and buildings were sorted out by applying a threshold to the magnitude of the residual of the spectral fit. From the spectral analysis the integrated NO$_2$ concentration along the atmospheric light path, the so-called slant column density (SCD) is derived. From this NO$_2$ SCD, the vertically integrated tropospheric NO$_2$ concentration, the so-called vertical column density (VCD) is derived using the so-called geometric approximation, which assumes direct absorption paths through the tropospheric NO$_2$ layer (Brinksma et al., 2008; Wagner et al., 2010). The uncertainty of the tropospheric NO$_2$ VCD derived in this way is typically below 25 % (Shaiganfar et al., 2011). For low tropospheric NO$_2$ VCDs, it is dominated by the fit error of the spectral analysis. For high tropospheric NO$_2$ VCDs it is dominated by the limitations of the geometric approximation depending on the Solar Zenith Angle (SZA), the relative azimuth angle, the NO$_2$ profile and the presence and properties of clouds. Close to strong emission sources, where the major fraction of NO$_2$ is located close to the surface, the errors caused by the geometric approximation are small (Shaiganfar et al., 2011). It is also important to note that – depending on the SZA and relative azimuth angle – the application of the geometric approximation can lead to an over- or underestimation of the
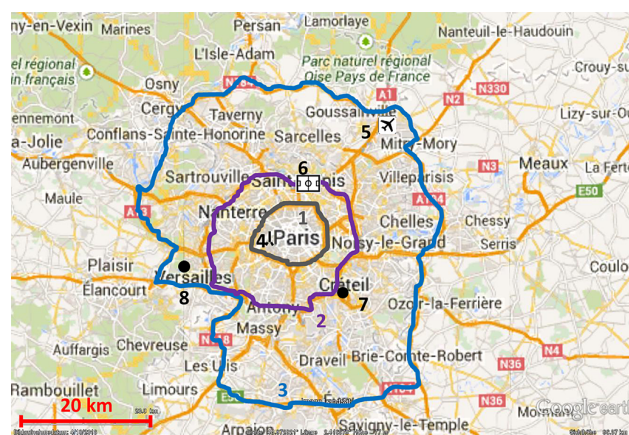

Figure 1. Typical driving routes around Paris with different radii. The numbers indicate the following – 1: small circle (Périphérique), 2: intermediate circle, 3: large circle, 4: Eiffel tower, 5: Airport, 6: Stade de France, 7: Creteil, 8: Palace of Versailles.

true tropospheric NO$_2$ VCD. Thus, since in this study we analyse a large number of individual car-MAX-DOAS measurements performed during several months in summer 2009 and winter 2009/2010, on average the uncertainties caused by the geometric approximation should mostly cancel out.

Different driving routes in and around Paris were used on different days (Fig. 1). On most days (34 days), measurements around large circles (Fig. 2a) were carried out, usually also including additional measurements closer to the city centre (Fig. 2b). On some days, measurements around smaller circles (Fig. 2c) or following different patterns (Fig. 2d) were also performed.

2.2 OMI

OMI was launched in 2004 onboard the Aura satellite (Levelt et al., 2006). It measures spectra of light scattered in the Earth's atmosphere and reflected by the Earth's surface. OMI covers the UV and visible spectral range up to 500 nm, enabling the DOAS retrieval of ozone, NO$_2$, and other minor trace gases.

Aura is operated on a sun-synchronous orbit, crossing the equator at 13:45 LT. Spatial resolution is 13×24 km^2 at nadir and decreasing towards the swath edges. Total swath width is 2600 km, resulting in daily global coverage. However, since 2007, so-called "row anomalies" lead to the dismissing of data for several cross-track positions (Boersma et al., 2011).

In this study, we use operational tropospheric NO$_2$ VCDs from the DOMINO data product v2.0 (Boersma et al., 2011). Based on the OMI standard NO$_2$ SCDs (Boersma et al., 2002), first the stratospheric column is removed by assimilation, and subsequently the tropospheric VCDs are derived based on a-priori vertical NO$_2$ profiles, both steps using the TM4 CTM with a longitude–latitude resolution of $3° \times 2°$.
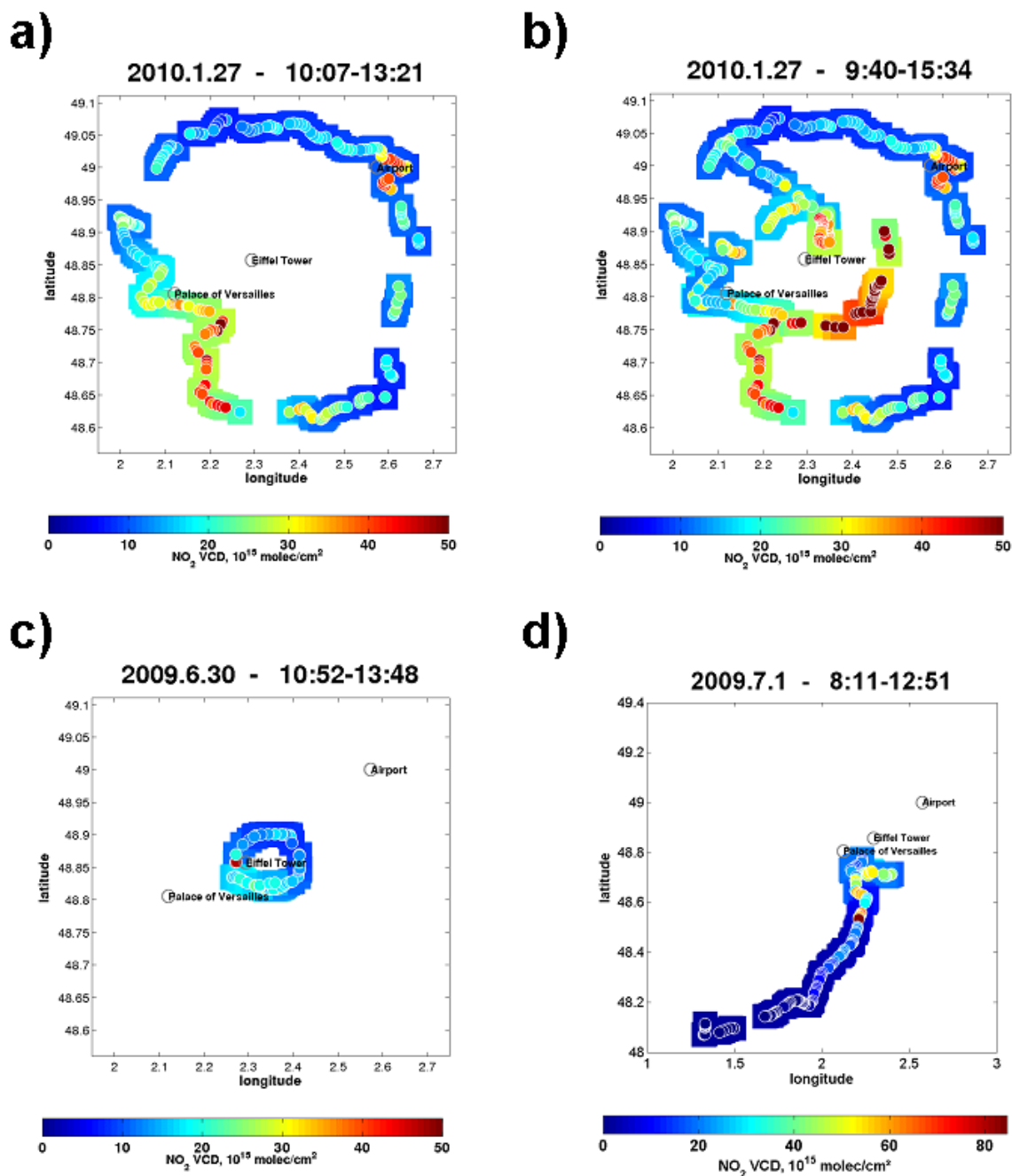
Figure 2. Typical car-MAX-DOAS results. **(a)** Measurements around large circles; **(b)** measurements around large circles and in the city centre; **(c)** measurements around small circles; **(d)** measurements at other road segments.

2.3 CHIMERE

In this paper, simulations are performed with the CHIMERE CTM (Schmidt et al., 2001; Menut et al., 2013) (www.lmd. polytechnique.fr/chimere) developed since 1997 by IPSL (Institute Pierre Simon Laplace) and INERIS (Institut National de l'Environnement Industriel et des Risques). The model is designed to produce daily forecasts of trace gases (e.g. O$_3$, NO$_x$) and aerosols (Honoré et al., 2008), as well as long-term (several years) simulations of emission control scenarios using different nesting possibilities (Beekmann and Vautard, 2010).

Simulations are performed with a horizontal resolution of 3×3 km^2 and a vertical discretization comprising eight vertical layers from ground to about 5 km, with decreasing vertical resolution with altitude.

Anthropogenic emissions input data are taken from the so-called TNO-MP (MEGAPOLI) European emission inventory built by the TNO in the framework of the MEGAPOLI project (Valari and Menut, 2008). It is based on the TNO inventory (Kuenen et al., 2014) but incorporates, over four megacities in Europe (Paris, London, Po valley, Rhine–Rhur region), bottom-up emission data compiled by local authorities (e.g. Airparif in Paris) (Timmermans et al., 2013). It is characterized by a high spatial resolution, $1/8° \times 1/16°$ longitude–latitude (roughly $7 \times 7\,km^2$). The activity and country specific diurnal (hourly) variations in emission rates are considered. They are applied during the emission pre-processing procedure (Menut et al., 2013). This inventory is described in more details in Kuenen et al. (2014), and have already been used in several studies (Zhang et al., 2013; Timmermans et al., 2013; Petetin et al., 2014). In addition, Paris NO$_x$ emissions from this inventory have been evaluated by Petetin et al. (2014), based on airborne measurements in the Paris plume during the MEGAPOLI summer campaign, showing a probable moderate positive bias (with a best estimation of $+29\,\%$). Biogenic emissions are computed based on MEGAN (Model of Emissions of Gases and Aerosols form Nature) emission factors and parameterisations from Guenther et al. (2006).

Meteorological data are produced with the PSU/NCAR Mesoscale Model (MM5; Dudhia et al., 1993). MM5 provides meteorological data for CHIMERE in an hourly time step. Observed wind speeds used for the comparisons are available at an hourly time step. In general, observed (and simulated) wind directions smoothly change form 1 hour to the next, at a rate of typically $10–20°$ (see Fig. 2 in Zhang et al., 2013). However, especially during low wind speed periods, much larger jumps in observations are possible, which are then often not simulated. In these cases however, the average transport time between NO$_x$ emission sources and the measurements is of several hours, which averages out sudden jumps in wind direction.

Boundary and initial conditions are taken from the LMDz-INCA2 and LMDz-AERO global models for gaseous and particulate species, respectively (Hauglustaine et al., 2004; Folberth et al., 2006). Land-use data are taken from the $1 \times 1\,km^2$-resolved GLCF (Global Land Cover Facility) global database (Hansen et al., 2000).

3 Advantages and limitations of the considered data sets

The three data sets differ in many aspects, the most important properties are discussed below.

3.1 Measured quantity

From the satellite and car-MAX-DOAS observations the tropospheric vertical column density (VCD) is derived, which is the vertically integrated NO$_2$ concentration in the troposphere. No detailed information on the vertical profile can be derived from these observations, because only high elevation angles (angles between the horizon and the viewing direction) are used. In contrast, the CHIMERE model provides three dimensional NO$_2$ concentrations fields from which NO$_2$ vertical columns can be directly calculated. It is worthwhile noting that the model does not extend beyond $\sim 5\,km$ above ground level, and thus does not cover the whole troposphere. However, as NO$_2$ is mostly located in the boundary layer (in particular close to megacities), the potential underestimation of tropospheric column is expected to be small. This is supported by the study of Konovalov et al. (2005) in which the partial tropospheric NO$_2$ column above 5 km has been estimated as about $0.5 \times 10^{15}\,mol\,cm^{-2}$ over the Paris region, thus less than about $10\,\%$. For the comparison with the car-MAX-DOAS measurements, the respective underestimation can be fully neglected, because the car-MAX-DOAS observations are only sensitive for atmospheric layers up to about 3 km (Frieß et al., 2006). Instead the NO$_2$ VCDs extracted from the model slightly overestimate the NO$_2$ VCDs retrieved from the car-MAX-DOAS measurements.

3.2 Spatial resolution

With typical measurement durations of about 1 min for an individual observation, the spatial resolution of the car-MAX-DOAS derived NO$_2$ distribution along the driving route is of the order of 1 km. In contrast, the horizontal resolution of the OMI observations is much coarser (at best $13 \times 24\,km^2$, see Sect. 2.2). The horizontal resolution of the CHIMERE simulation is 3 km.

3.3 Spatial coverage

For most days the measurement strategy was to drive around Paris along large circles (with diameters of about 35 km, see Fig. 3), in order to estimate the total emissions from Paris (Shaiganfar et al., 2011, 2015). Such measurements were carried out once or twice per day. In addition, measurements along smaller circles, and other road segments were performed on individual days to gain more information on the horizontal NO$_2$ distribution in the Paris metropolitan area. The satellite provides daily global coverage. However, on many days gaps in the tropospheric NO$_2$ data are present, due to the presence of clouds or instrumental problems. CHIMERE simulations are performed over an area ranging from $0.35°$ W to $4.41°$ E and $47.45–50.66°$ N.

3.4 Temporal coverage

OMI satellite observations over the Paris region are made once per day at around 13:45 local time (LT). Car-MAX-DOAS observations were typically made several times per
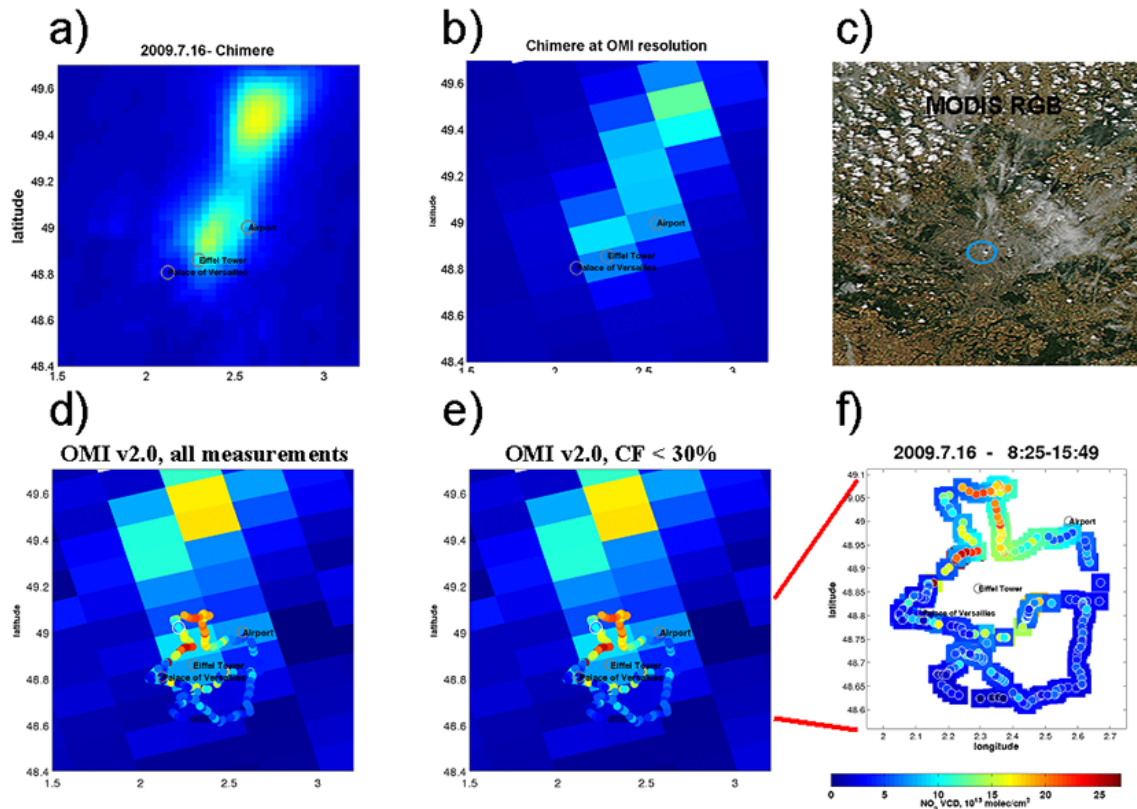
Figure 3. Comparison of the tropospheric NO2 VCDs across the Paris metropolitan area derived from model simulations, satellite observations and car-MAX-DOAS observations on 16 July 2009. **(a)** CHIMERE model results at the time of the OMI overpass (12:54) at original resolution; **(b)** CHIMERE results averaged for the individual OMI ground pixels; **(c)** MODIS RGB image; **(d)** OMI v2.0 data together with car-MAX-DOAS results; **(e)** same as **(d)** but for cloud fraction below 30 %; **(f)** car-MAX-DOAS results (small circles) together with CHIMERE model results extracted for the same time and location of the car-MAX-DOAS data (large squares). The car-MAX-DOAS measurements were performed between 8:25 and 15:49; the measurements around the large circle were performed between 10:07 and 14:05.

day between about 8:00 and 17:00 LT. CHIMERE data are available in hourly time steps.

3.5 Sensitivity and uncertainties

The measurement sensitivity of the car-MAX-DOAS and satellite measurements is systematically different: car-MAX-DOAS observations are most sensitive for layers close to the surface and become increasingly insensitive for altitudes above about 3 km (Frieß et al., 2006). In contrast, the sensitivity of satellite observations decreases towards the surface. This is accounted for in the satellite NO$_2$ data product used in this study (the "Derivation of OMI tropospheric NO$_2$ (DOMINO)" product, see Sect. 2.2) based on (relative) a-priori vertical NO$_2$ profiles from the TM4 CTM. However, especially close to strong emission sources, the model profiles can differ strongly from the true NO$_2$ profiles. Here it is important to note that the uncertainty of the actual NO$_2$ profile usually constitutes the major uncertainty for satellite retrievals of tropospheric NO$_2$ VCDs. The typical uncertainties of the car-MAX-DOAS and satellite measurements are

about 25 % (Shaiganfar et al., 2011) and 35–60 %, respectively (Boersma et al., 2004).

The uncertainties of the model data depend on several input parameters, in particular the distribution and strength of the individual emission sources, as well as chemical transformations and atmospheric transport play important roles. The orientation and the extent of the simulated emission plume depend critically on wind direction and speed, respectively.

3.6 Effects of clouds

The sensitivity of satellite observations for tropospheric trace gases is strongly influenced by clouds. In particular if a trace gas is located below a cloud layer, the satellite observations can become almost insensitive. The details of the cloud influence depend on the cloud properties, especially on the cloud fraction (CF) and cloud altitude. To minimise the cloud influence, often only measurements for small CF are considered. Here only OMI measurements with effective CF below 30 % are retained. In contrast to satellite observations, the sensitivity of car-MAX-DOAS measurements is hardly affected

by clouds as long as the trace gas is located below the cloud layer (which is a valid assumption close to strong NO$_x$ emission sources).

In summary, the characteristics of the three data sets are quite different; all three data sets have their specific strengths and weaknesses. The main limitations of the satellite observations are their coarse resolution, their large uncertainties, and their strong dependence on cloud cover and the a-priori assumptions on the NO$_2$ profile. The main limitations of the car-MAX-DOAS observations are their limited spatial and temporal coverage. Also the accuracy of the model data is limited by various uncertainties in emissions, chemistry and transport (e.g. Boynard et al., 2011).

The main aim of this study is to test the consistency of the three data sets during the two MEGAPOLI measurement campaigns in summer 2009 and winter 2009/2010. The most direct and usually applied way is the comparison of the original data sets. In addition to these basic comparisons, we also compare modified versions of the three data sets making synergistic use of the strengths and weaknesses of the three different data sets. Here modifications of the model data are of particular importance, because (i) the model results depend critically on the used input data, especially the wind fields and the distribution and strength of the emission sources, and (ii) the model data play a crucial role as transfer tool to connect both remote sensing data.

The following corrections to the original data sets are applied in this study.

a. The satellite and ground-based observations are used to test if the horizontal patterns of the pollution plumes in the CHIMERE simulation are correct. Possible mismatches in the direction of the emission plume (due to inaccurate wind direction in meteorological input data) are corrected by rotating the modelled concentration fields around the centre of Paris (see Sects. 4.1 and 5.2).

b. The car-MAX-DOAS data are used to test to which detail the model data can resolve the measured horizontal gradients. Different degrees of spatial smoothing are applied to the car-MAX-DOAS data until best match with the model data is achieved (see Sect. 4.2).

c. The vertical profiles extracted from the CHIMERE model data are used to improve the satellite retrievals. Compared to the results from the global model used in the original satellite product, the regional CHIMERE model resolves finer spatial gradients (see Sect. 5.1).

Here it should be noted that in cases when rotated CHIMERE data are used (see point a. above), not the original but the rotated CHIMERE profiles are applied to the OMI retrieval. This is an important detail, as the NO$_2$ profiles vary strongly depending on whether they are inside or outside the emission plume.

In addition, the car-MAX-DOAS data and model results are used for satellite validation with a specific focus on the effects of clouds on the satellite retrievals (see Sects. 5 and 6). And the satellite and model data are used to investigate the representativeness of the car-MAX-DOAS data. The model data are used as a transfer tool to bridge the different scales of the MAX-DOAS and satellite observations (see Sect. 6).

Typical examples for the comparison of the three data sets during the Paris campaigns are illustrated in Figs. 3 and 4. Besides the original model data (at 3×3 km^2 resolution), the re-gridded model data matching the spatial resolution of the satellite observations are also shown. Car-MAX-DOAS results are displayed in the plots of the satellite data and separately in a zoomed image (also showing the results of the CHIMERE model). Figure 3 represents a day with almost ideal conditions for the comparison of the different data sets: the satellite covers the whole Paris metropolitan region and only few clouds are present (CF is below 30 % for all satellite pixels). Paris is close to the centre of the swath of the OMI orbit; thus the size of the satellite ground pixels is rather small. The car-MAX-DOAS observations cover several OMI ground pixels. Enhanced values of the tropospheric NO$_2$ VCDs are found at similar locations in all three data sets. However, the pattern of the simulated plume does not exactly match the satellite and car-MAX-DOAS observations: compared to the measurements the model plume is slightly rotated counterclockwise (by about 15°). This discrepancy is likely mostly due to inaccuracies in the simulated wind fields, and in particular the wind direction. Figure 4 represents a day with similar conditions, but on that day a field of broken clouds was present over the Paris metropolitan region. While for many of the satellite observations the effective CF is still below 30 %, no enhanced NO$_2$ VCDs are seen in the satellite data (in contrast to the model data and car-MAX-DOAS measurements). This indicates a strong shielding effect of the clouds for the satellite observations of that day. Here it is important to note that usually for low CF the satellite retrievals yield reasonable tropospheric NO$_2$ VCDs. However, close to strong emission sources, the shielding effect of clouds depends critically on the relative locations of the clouds and the areas of enhanced NO$_2$ concentrations. If e.g. a cloud patch covers an area of high tropospheric NO$_2$, the satellite data are biased low. If instead the cloud patch covers areas of low tropospheric NO$_2$, the satellite data are hardly affected by the clouds.

The comparison of the car-MAX-DOAS and model data presented in Fig. 4 again indicates a spatial mismatch between both data sets: the model data would have to be rotated counterclockwise by about 25° to match the car-MAX-DOAS measurements.

In this paper we compare the three data sets in a quantitative way for all days with available car-MAX-DOAS measurements. In addition to the original data sets we compare versions which are modified in different ways as indicated above and described in detail in the respective sections. An overview of the different modifications is presented in Table 1.
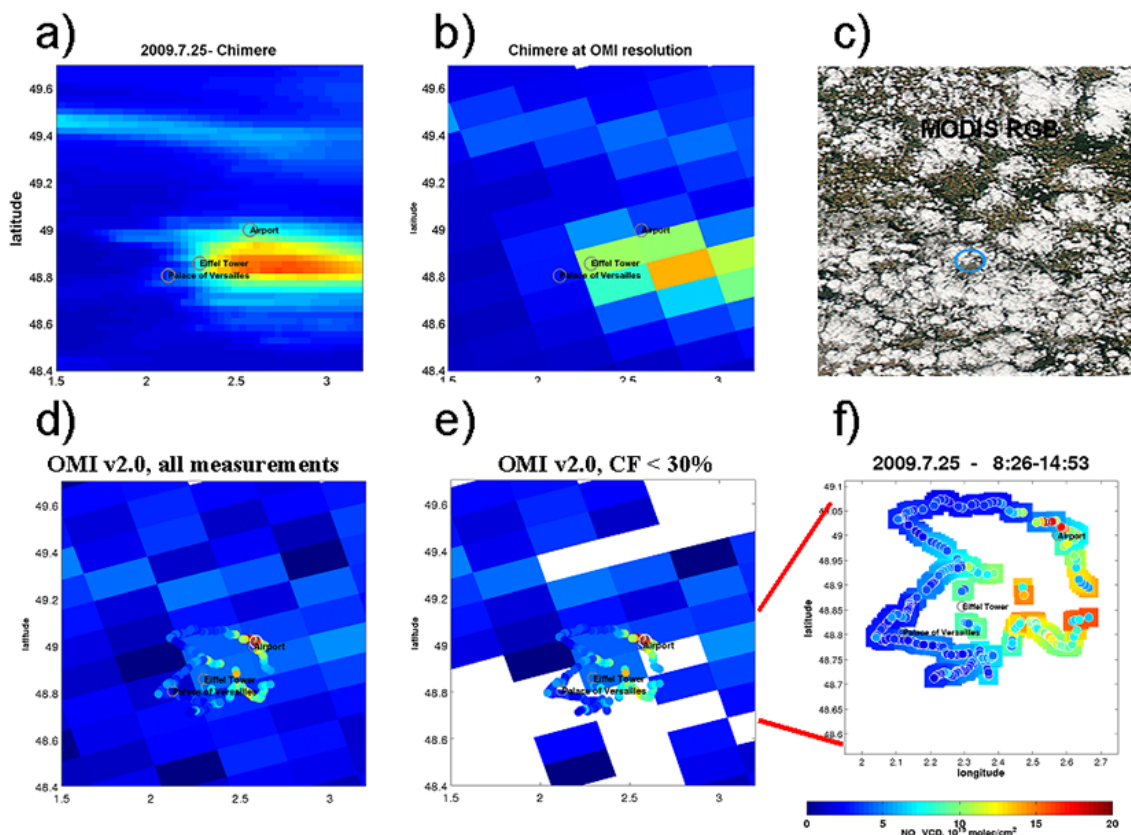
Figure 4. Same as Fig. 3 for the 25 July 2009. OMI overpass was on 12:47; the car-MAX-DOAS measurements were performed between 8:26 and 14:53; the measurements around the large circle were performed between 11:37 and 14:07.

Table 1. Overview on the different quantities used in this study.

| Quantity	Description
Original car-MAX-DOAS data	Tropospheric NO$_2$ VCDs for a given off-zenith elevation angle, determined using the geometric approximation.
Smoothed car-MAX-DOAS data	Horizontally smoothed tropospheric NO$_2$ VCDs using Gaussian functions with sigma values of 6 and 8 km for summer and winter, respectively.
Scaled car-MAX-DOAS data	Average of smoothed car-MAX-DOAS data over an OMI pixel divided by the ratio of CHIMERE(DOAS)/CHIMERE(OMI).
Original CHIMERE data	Vertically integrated NO$_2$ concentrations (tropospheric NO$_2$ VCD) for a 3 km × 3 km CHIMERE grid.
Rotated CHIMERE data	CHIMERE data rotated around the centre of Paris to match the car-MAX-DOAS or OMI data.
CHIMERE(DOAS)	(rotated) CHIMERE data averaged for the locations of all car-MAX-DOAS inside an OMI pixel.
CHIMERE(OMI)	(rotated) CHIMERE data averaged over the whole OMI pixel.
Original OMI data	Tropospheric NO$_2$ VCD derived from OMI observations (DOMINO product, v2.0).
Modified OMI data	Tropospheric NO$_2$ VCD derived from OMI observations using the NO$_2$ profile from rotated CHIMERE instead of the TM-4 model.
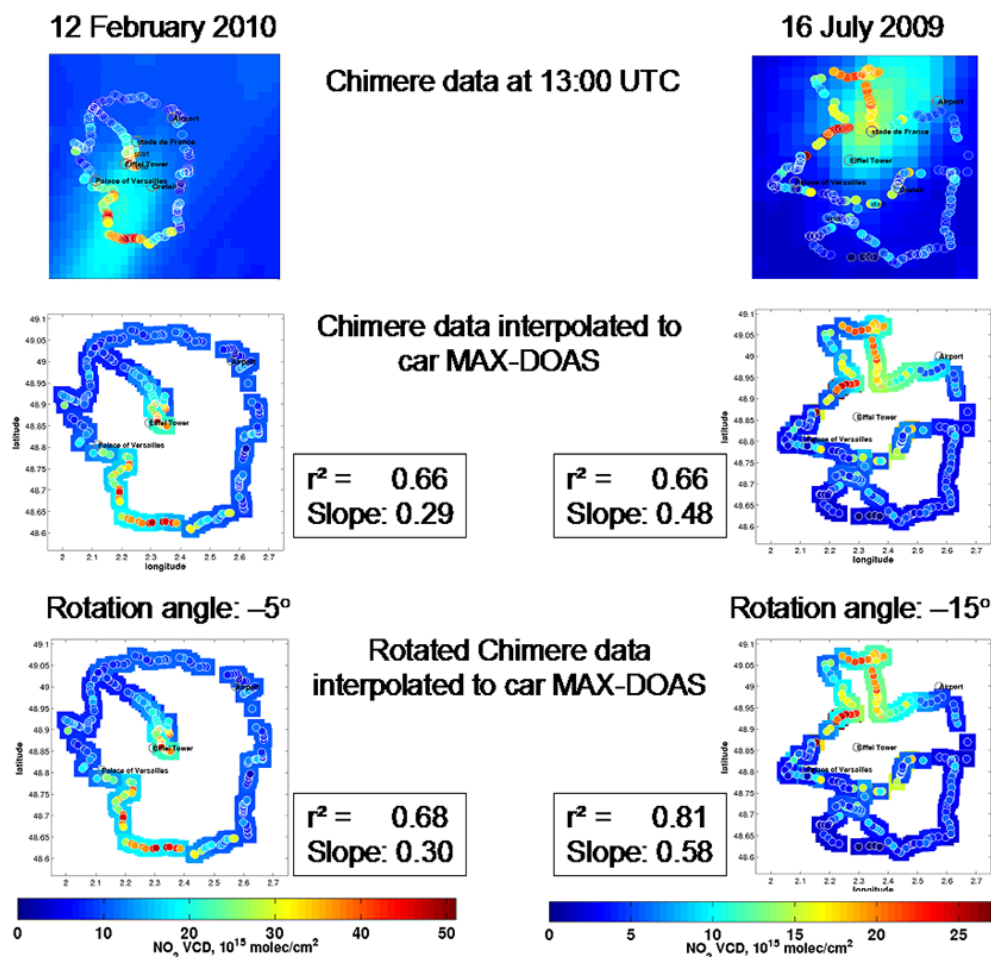
Figure 5. Comparison of car-MAX-DOAS observations with model results for 12 February 2010 (left) and 16 July 2009 (right). Top: CHIMERE data at the centre time of the car-MAX-DOAS observations (13:00); middle: CHIMERE data interpolated in space and time to match the individual car-MAX-DOAS observations; bottom: rotated CHIMERE data interpolated to the car-MAX-DOAS observations.

4 Comparison between CHIMERE and car-MAX-DOAS

4.1 Spatial patterns and horizontal rotations of the model data

Comparison of the spatial distribution of NO$_2$ from the CHIMERE model and car-MAX-DOAS measurements generally shows similar spatial patterns, but often reveals a small "tilt" between both data sets. Here we illustrate this effect and show that correlations between both data sets can be significantly improved if the model data are rotated. Possible reasons for the tilt are discussed below. Figure 5 shows comparisons between car-MAX-DOAS observations and the CHIMERE results for 2 selected days (12 February 2010 and 16 July 2009). The identical car-MAX-DOAS data are displayed in all sub-figures, but for CHIMERE, different versions are shown. The top panel presents the horizontal distribution of the simulated tropospheric NO$_2$ VCDs

across the entire area at 13:00 UTC, the approximate median times of the car-MAX-DOAS observations on both days (16 July: 8:25–15:49 UTC; 12 February: 9:57–15:22 UTC). In the middle panel, CHIMERE data are interpolated to the exact times and locations of the individual car-MAX-DOAS observations (coloured squares in the background). On both days different levels of agreement are found: for 12 February 2010 (left) the spatial patterns of the car-MAX-DOAS measurements and CHIMERE data match quite well, but the absolute values differ. On 16 July 2009 both absolute values and spatial patterns differ.

In the lower panel of Fig. 5 the CHIMERE data are rotated around the centre of Paris. The rotation angle was determined by optimising the spatial correlation between the car-MAX-DOAS observations and the CHIMERE data (rotation angles are varied in steps of 5° between ±25°). On 12 February 2010 the best agreement was found for a small rotation angle (−5°) whereas on 16 July 2009, the best agreement was found for a larger rotation angle of −15°. After ap-
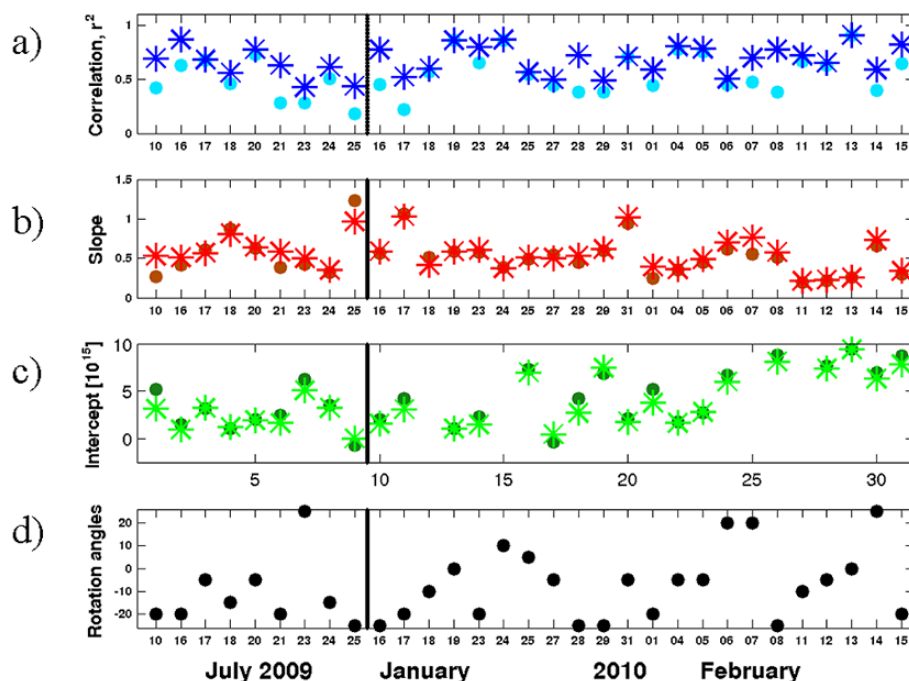
Figure 6. Results of the spatial correlation analyses between CHIMERE and car-MAX-DOAS for individual days (dots: results for original CHIMERE data; stars: results for rotated CHIMERE data). **(a)** Correlation coefficients; **(b)** slopes of the regression lines; **(c)** *y* axis intercepts; **(d)** optimum rotation angles.

plying the rotations, the agreement of the spatial patterns improved substantially: for 16 July 2009, the correlation coefficient (r^2) increased from 0.66 to 0.81 and the slope increased from 0.48 to 0.58. On 12 February 2009 the influence of the (small) rotation was smaller (r^2 changed from 0.66 to 0.68; the slope changed from 0.29 to 0.30).

We applied rotations to CHIMERE data for all days when car-MAX-DOAS measurements around large circles are available. We chose car-MAX-DOAS measurements around large circles, because these observations allow the most accurate determination of the emission plume of Paris. Here it should be noted that instead of rotating the model results, it would have been more correct to rotate the wind fields before using them in the model simulations (and leaving the emissions sources unchanged). However, this procedure would be very time-consuming, since complete model simulations would have to be performed for each rotation angle of the wind fields. Fortunately, for the model results the errors caused by rotating the whole wind fields are small, because the NO$_x$ emissions within the Paris agglomeration (within about 20–30 km distance from the Paris centre) are on the average about 2 orders of magnitude larger than emissions outside the agglomeration (see Fig. 1c, Petetin et al., 2014). The next larger cities (Orléans, Reims, Rouen) are at more than 100 km distance from the agglomerations, but their population is much smaller (100 000–200 000 inhabitants) than that of the Paris agglomeration (nearly 12 million inhabitants). Outside the Paris agglomeration, emissions

are concentrated along several highways as well as along the Seine and Marne rivers. But again, these emissions are much smaller than those within the agglomeration. Here it should be noted that for many other cities, probably less ideal conditions exist. In such cases, modified rotation methods might be applied, by e.g. excluding areas with strong interfering sources outside the city centre.

The results of the spatial correlation analyses for the original and rotated CHIMERE data are shown in Fig. 6. The applied rotations cause a substantial improvement of the correlation coefficients. While such an improvement has to be expected (and was the criterion to determine the rotation angles), it is interesting to note that also the slopes of the regression lines increase while the *y* axis intercepts decrease. However, the slopes are still systematically smaller than unity, and the *y* axis intercepts are larger than zero, indicating an underestimation of the maximum NO$_2$ VCDs and overestimation of the background NO$_2$ VCDs by CHIMERE.

In Fig. 7 we show correlation plots between CHIMERE and car-MAX-DOAS data for 2 selected days: on 16 July 2009 (top) the correlation is largely increased for the rotated CHIMERE data; on 27 July 2009 similar correlation is found for original and rotated CHIMERE data. On both days the slope is close to 0.5 and is hardly affected by the rotation of the CHIMERE data.

The frequency distribution of the optimum rotation angles is presented in Fig. 8. There, in addition to the results of the comparison to the car-MAX-DOAS data, the corresponding
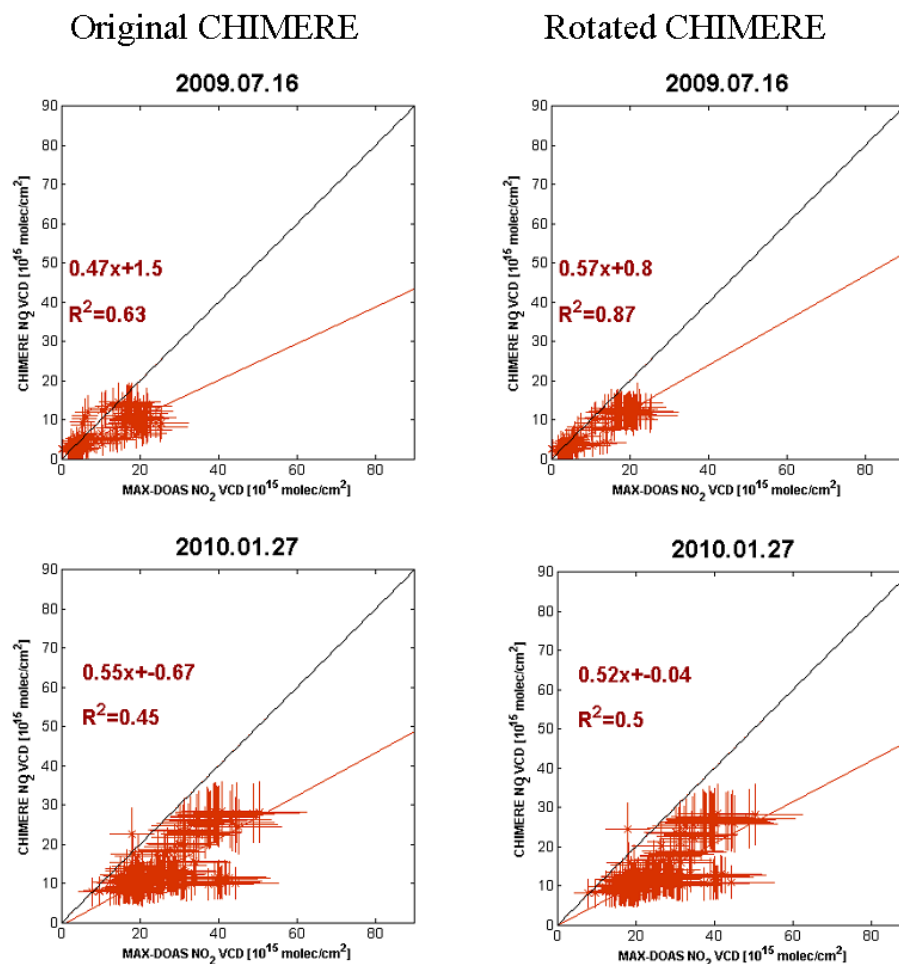
Figure 7. Correlation analyses of original (left) and rotated (right) CHIMERE data versus coincident car-MAX-DOAS observations for 2 selected days. On 16 July 2009 (top) the rotation substantially improves the correlation. On 27 January 2010, the rotation only leads to a slightly improved correlation.

results for the comparison to the OMI observations are also shown (note that in contrast to Fig. 6 not only measurements around large circles are shown). Somewhat different rotation angles are found for the comparison between car-MAX-DOAS and OMI observations with a correlation coefficient $r^2 = 0.28$ between both sets of the rotation angles. The rather low correlation is probably caused by the fact that the comparisons of the model data with both observational data sets are made for different times and locations. In particular the comparisons versus OMI observations are performed for a much larger area (see Figs. 3 and 4).

From the comparison of CHIMERE data to both observational data sets counterclockwise rotations are found more frequently than clockwise rotations, with corrections reaching up to 25°. Such differences between simulated and observed surface wind direction of this order are frequently observed for surface winds (at 10 m height) at the SIRTA site at Ecole Polytechnique, Palaiseau, at 20 km SW from the town centre. This site is chosen, because it delivers observations
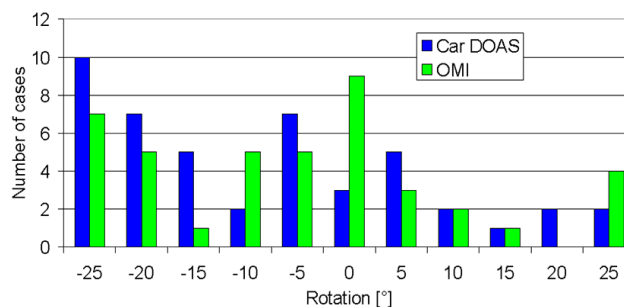

Figure 8. Frequency distribution of the optimum rotation angles for the comparison of the CHIMERE data with car-MAX-DOAS observations (blue) and satellite observations (green). Here not only results for large circles (like in Fig. 6), but for all measurements are shown.

of meteorological and dynamical parameters of high quality and with a known spatial representativity (Haeffelin et al.,
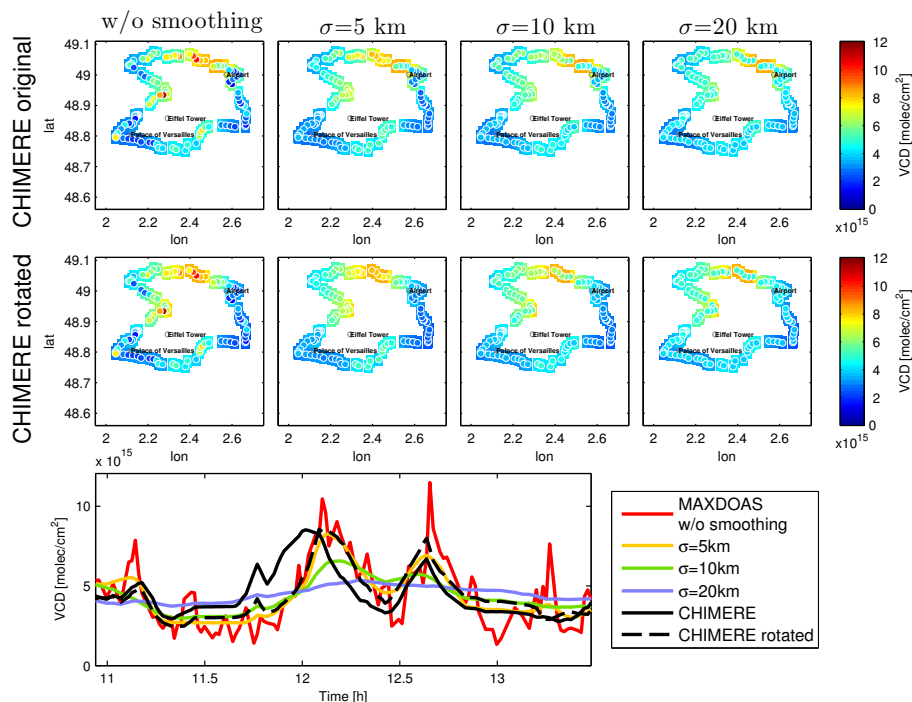
Figure 9. Top: comparison of the car-MAX-DOAS results (small circles) with coincident original or rotated CHIMERE results (squares) for 21 July 2009. The different plots present car-MAX-DOAS data smoothed by Gaussian functions with different smoothing kernels (σ ranging from 0 to 20 km). Bottom: the same data presented as function of time.

2005). The measurement site is located on a plateau and in mostly free terrain. For July 2009 (covering most of the summer measurement period in this paper), wind direction errors were generally below $\pm 20°$ (except for days with very low wind speed below $2\,\mathrm{m\,s^{-1}}$) (Zhang et al., 2013). These errors are compatible with the typical mesoscale model errors on one hand (Pielke et al., 2013), and with the optimal rotation angles found in our study, on the other hand. The interesting feature about the present comparison from pollution tracer data is that it horizontally integrates differences over the whole transport distance between emission sources and the measurement location, and vertically over the effective depth of vertical mixing. An interesting indication from this study is that there could be a bias in this effective transport direction.

4.2 Influence of spatial smoothing of the car-MAX-DOAS data

In addition to the rotation of the CHIMERE data we also investigated if the nominal resolution of the CHIMERE data matches the spatial gradients observed by car-MAX-DOAS. For that purpose we applied a spatial smoothing (convolution with Gaussian kernels of different widths) to the car-MAX-DOAS results before they are compared to the CHIMERE data. Two of these comparisons are shown in Figs. 9 and 10. Both days were chosen because they represent cases of dif-

ferent improvement after the application of smoothing and rotation. On 21 July 2009 (Fig. 9) best agreement between both data sets is found after the car-MAX-DOAS data are smoothed with a kernel of 4 km (in addition to a rotation of $-20°$). On 24 January 2010 (Fig. 10) best agreement is found if smoothing kernels between 8 and 12 km are applied (together with a rotation of 10°). But on that day systematic differences remained even after applying both modifications.

An overview on the effect of the spatial smoothing for all days is presented in Fig. 11. The results of the correlation analyses (top: correlation coefficients r^2; middle: y axis intercepts; bottom: slopes) are displayed as a function of the width of the applied smoothing kernel. The thin lines indicate the results for the individual days, and the thick lines indicate the averages of all days. For both original and rotated CHIMERE data best agreement (highest correlation coefficients and slopes closest to unity) is found after smoothing the car-MAX-DOAS data with kernels of 5 km or larger. As expected, much more consistent results are found for the comparison with the rotated CHIMERE data (right panel), because without rotation the possible mismatch between both data sets often prevents a meaningful comparison. For the rotated CHIMERE data the optimum smoothing kernels are slightly larger in winter than in summer.

Interestingly, the optimum horizontal smoothing kernels are significantly larger than the spatial resolution of the CHIMERE data (3 km). This result was unexpected, and the
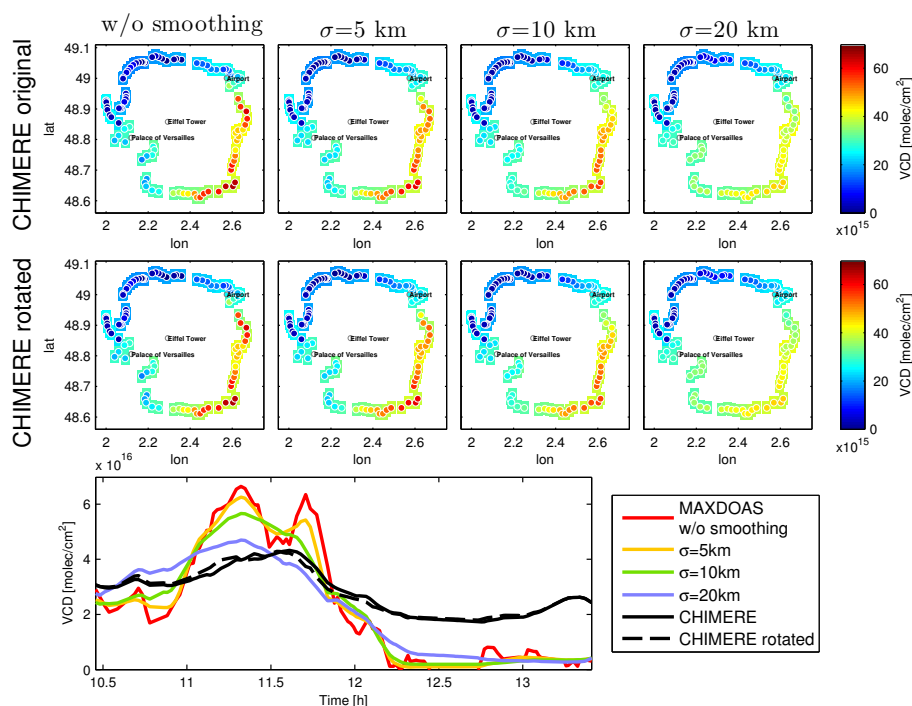
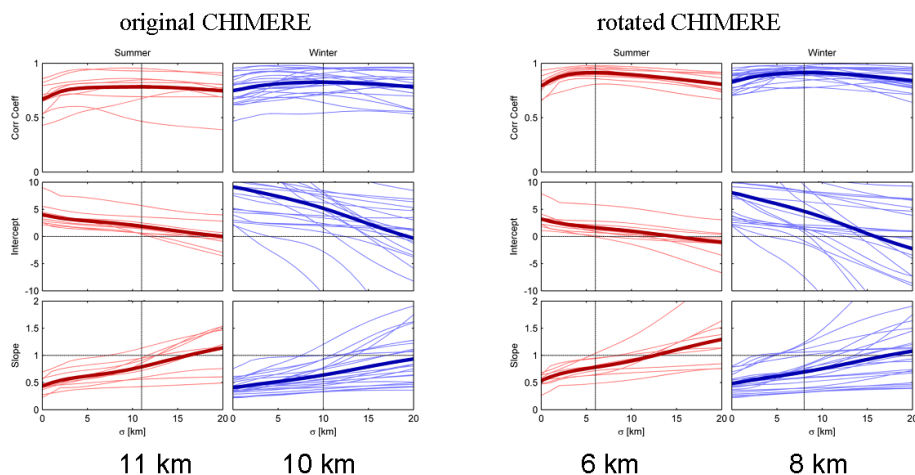**Figure 10.** Same as Fig. 9, but for 24 January 2010.

Figure 11. Results of the spatial correlation analyses between CHIMERE and car-MAX-DOAS data for individual days (thin lines) as function of the smoothing kernel (measurements along large circles). The thick lines indicate the averages of the individual days. Left: original CHIMERE data; right: rotated CHIMERE data. The vertical lines indicate the smoothing kernels, for which the highest correlation coefficients are found.

potential reasons for the need of an additional smoothing are not completely clear. Probably some atmospheric process(es) relevant for the dispersion of the NO_2 plume are not sufficiently well represented in the model. Such processes might include atmospheric mixing but also the characteristic times of chemical reactions. Alternatively, also the spatial distribution of the emission sources used in the model simulations might be too coarse, or their spatial emission distribution might be imperfect at small scales of some kilometres. In addition sampling effects and numerical diffusion might also contribute. In all these cases, smoothing of the spatial scales reduces model errors and improves comparison with observations. A similar result was found by Valari and Menut (2008). They found that smoothing of pollutant emissions to 12 km horizontal resolution gave best results for comparison of CHIMERE simulations over Paris with ob-

Table 2. Ratios of daily average and maximum values (CHIMERE/car-MAX-DOAS) as well as slopes and correlation coefficients of the regression analyses for measurements at large circles.

Quantity	Ratio CHIMERE/original car-MAX-DOAS		Ratio CHIMERE/smoothed car-MAX-DOAS	
	Summer	Winter	Summer	Winter
Ratio of averages	1.01	0.86	1.01	0.87
Ratio of maxima	0.59	0.53	0.94	0.75
Slope (r^2)	0.61 ($r^2 = 0.63$)	0.52 ($r^2 = 0.47$)	0.70 ($r^2 = 0.77$)	0.64 ($r^2 = 0.54$)

served surface ozone (for the case of observed ozone values above the 90 ppb information threshold). This again points to the fact that model processes at smaller scales are probably not well enough represented in the chemistry transport model or its input data.

Figure 12 presents a comparison of the daily average and maximum values of the tropospheric NO$_2$ VCDs from car-MAX-DOAS and CHIMERE. The maximum values were determined, taking into account data at the locations of the individual car-MAX-DOAS measurements.

The tropospheric NO$_2$ VCDs show a considerable variation from day to day, which is well represented in both data sets. For the daily averages (Fig. 12a), the smoothing of the car-MAX-DOAS data has almost no effect (as expected). But the daily maxima of the car-MAX-DOAS observations (Fig. 12b) strongly decrease after the smoothing is applied. Furthermore, the agreement between CHIMERE and car-MAX-DOAS results is largely improved after the smoothing. The averaged daily ratios of maximum and average values are summarised in Table 2. The ratios of the averages for the original and smoothed car-MAX-DOAS data are about 1.01 and 0.87 for summer and winter, respectively, indicating good agreement between both data sets in summer and a systematic underestimation of the car-MAX-DOAS data by CHIMERE in winter. The ratios of the daily maxima increase after smoothing from 0.59 to 0.94 in summer and from 0.53 to 0.75 in winter. Despite this considerable improvement, especially in winter, the CHIMERE model systematically underestimates the tropospheric NO$_2$ VCDs in the Paris plume by about 25 %. In Fig. 13 correlation results for the whole summer and winter campaign data sets of individual car-MAX-DOAS measurements versus the coincident CHIMERE values are presented for the original and modified data sets. The correlation analyses are performed by an orthogonal linear regression (Cantrell, 2008) because this type of regression analysis, allows considering uncertainties of both compared data sets. The errors of the car-MAX-DOAS measurements are described by a constant (2×10^{15} molec cm^{-2}) and a linear term (20 %) (see Shaiganfar et al., 2011). Since for the CHIMERE data no error is provided, we simply used the same errors as for the car-MAX-DOAS measurements. Of course, the choice is arbitrary, but it is only technical in order to perform the linear regression.
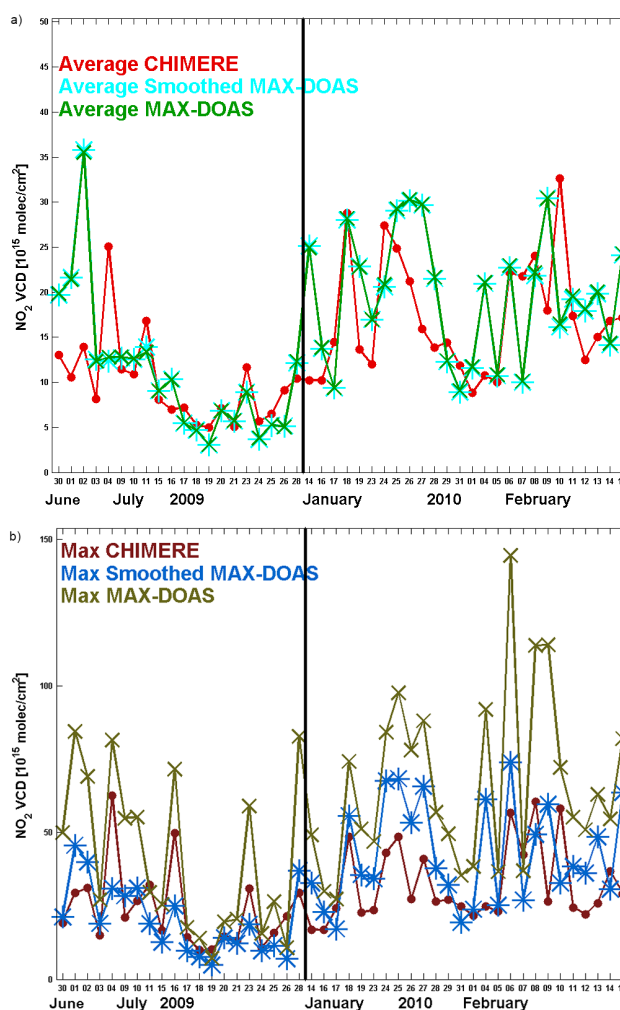
Figure 12. Comparison of the daily average **(a)** and maximum **(b)** tropospheric NO$_2$ VCDs for original and smoothed car-MAX-DOAS observations (all data) and coincident CHIMERE data.

The exact value of the assigned uncertainties only little affects the results of the fit. Unambiguously assigning uncertainties to modelling results is difficult, because for instance differences to observations are always affected by representativeness and measurement errors. The correlation results improve systematically after both modifications, i.e. rotation
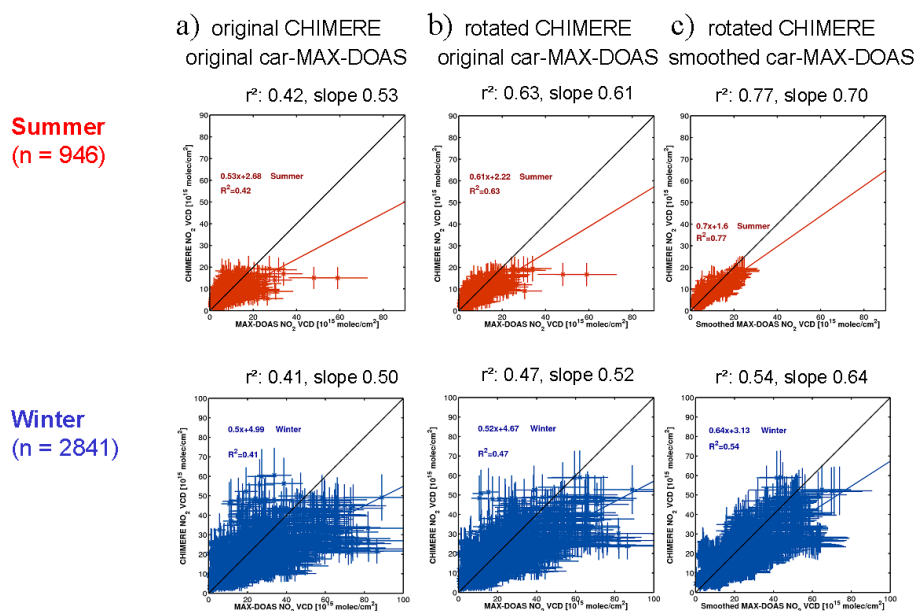
Figure 13. Correlation analyses between CHIMERE and car-MAX-DOAS observations (along large circles) for **(a)** the original data sets, **(b)** rotated CHIMERE data, and **(c)** rotated CHIMERE data and smoothed car-MAX-DOAS data.

of CHIMERE data and spatial smoothing of car-MAXDOAS data, with larger improvements in summer. However, still the slopes remain smaller than unity (0.77 in summer and 0.64 in winter) and the y axis intercepts larger than zero.

4.3 Quantitative interpretation of the comparison results

We quantify the agreement of the tropospheric NO₂ background VCDs based on the ratios of the daily average values of CHIMERE versus car-MAXDOAS (Fig. 12a). For summer, the ratios both for the original and smoothed car-MAX-DOAS data are close to unity (see Table 2), indicating good agreement between both data sets. In contrast, for winter the ratios are lower (0.86 and 0.87 for the original and smoothed car-MAX-DOAS data, respectively), indicating that CHIMERE probably systematically underestimates the car-MAX-DOAS measurements. Here it is, however, interesting to note that this discrepancy is within the measurement uncertainty of the car-MAX-DOAS observations (see Sect. 2.1).

The agreement of the tropospheric NO₂ VCDs of the emission plume are quantified by the ratios of the daily maxima (Fig. 12b) and the slopes of the regression lines of the individual data pairs (Fig. 13). For the original car-MAX-DOAS data the ratios and slopes are between 0.59 and 0.61 and between 0.52 and 0.53 for summer and winter, respectively. If the smoothed car-MAX-DOAS data are considered, the ratios and slopes are much closer to unity: they are between 0.70 and 0.94 and 0.64 and 0.75 in summer and winter, re-

spectively. But they still indicate a strong and systematic underestimation by CHIMERE.

Here it should be noted that similar results are found if in addition to the measurements along the large circles also the measurements in the city centre on the same days are considered (Fig. S1a in the Supplement). Also for all coincident measurements similar results are obtained (Fig. S2), but the correlations become worse, because in many cases the rotation angle of the CHIMERE data is less well constrained than for the large circles. Note that for larger smoothing lengths (higher sigma), slopes close to 1 and intercepts close to 0 can be reached (Fig. 11), while correlation coefficients again decrease. However, for lengths above 10 km, the Paris emission plume becomes less and less resolved.

5 Comparison between CHIMERE and OMI

5.1 Influence of the selected NO₂ profiles on the satellite data

The tropospheric NO₂ VCD retrieved from OMI depends systematically on the (relative) NO₂ profile used in the inversion process (Boersma et al., 2011). For the OMI version used in this paper (DOMINO v2.0) the NO₂ profiles are taken from the TM4-model (Boersma et al., 2007, 2011), which has a spatial resolution of 2° in latitudinal and 3° in longitudinal direction. It has 34 vertical layers below 0.38 hPa with the vertical resolution of the lowest layer of about 25 m. Due to the rather coarse horizontal resolution, the model is probably not capable of resolving spatial gradients close to strong emission sources. In particular, in such cases the simulated
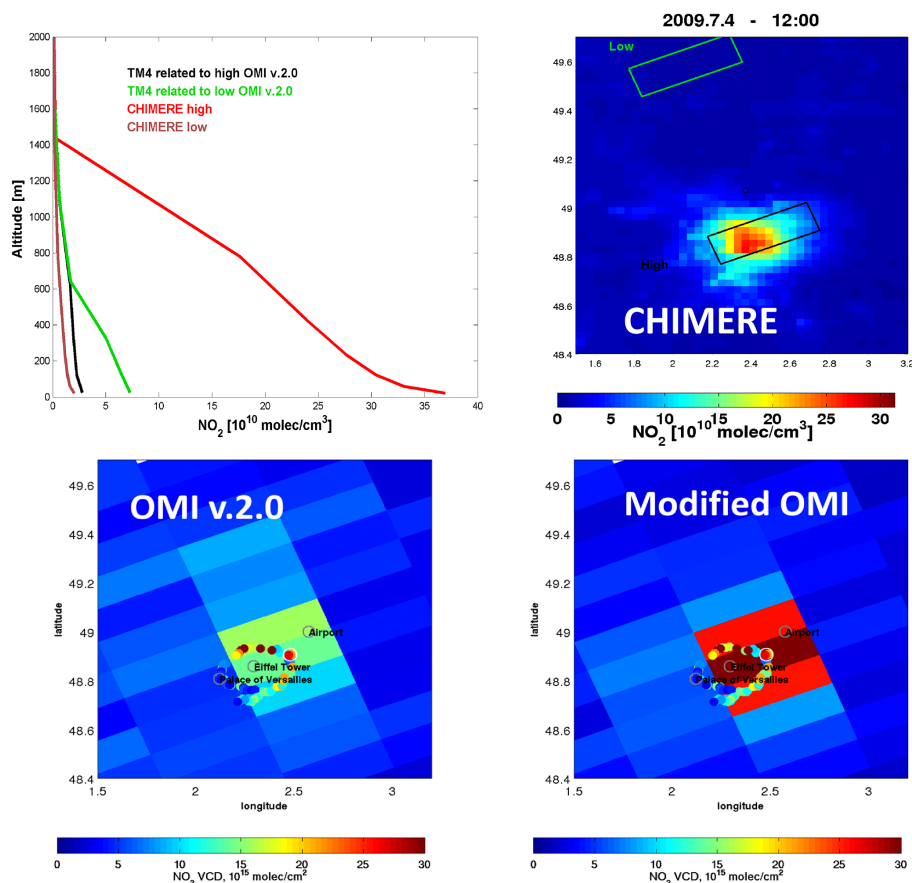
Figure 14. (a) Comparison of the vertical NO₂ profiles from TM-4 and CHIMERE for locations inside or outside the emission plume on 4 July 2009; **(b)** near-surface (0–44 m) NO₂ concentrations from CHIMERE and locations of the selected profiles; **(c)** OMI results from the operational product (v2.0); Modified OMI results using the NO₂ profiles from the regional CHIMERE model.

NO₂ profiles probably underestimate the enhanced concentrations close to the ground. To investigate the influence of the NO₂ profile on the OMI results in more detail we compared the NO₂ profiles from the TM-4 model over Paris with the corresponding profiles from the CHIMERE model (with a much higher spatial resolution of $3 \times 3\,\mathrm{km}^2$) for selected OMI observations. In Fig. 14 NO₂ profiles in the Paris plume and for "background" levels are shown for 4 July 2009. For the OMI pixel in the plume, the CHIMERE profile shows much higher NO₂ concentrations for altitudes < 1 km than the TM-4 model. Replacing the TM-4 profiles by the CHIMERE profiles in the satellite data retrieval leads to smaller air mass factors and thus to higher tropospheric NO₂ VCDs: for the measurements of the emission plume shown in Fig. 14 the tropospheric NO₂ VCD increases by about a factor of 2. In contrast, for measurements outside the emission plumes the values hardly change. Similar results are found for the other measurement days.

Thus in all further comparisons of this study, in addition to the original DOMINO v2.0 product, we also consider the

OMI results retrieved using the CHIMERE profiles (this version is referred to as modified OMI data).

Here it is important to note that, the modified OMI data are partly dependent on the CHIMERE profiles. In an extreme case, for example, the application of CHIMERE profiles to a hypothetic homogenous (non-zero) OMI NO₂ field would cause a deceptive high correlation between OMI and CHIMERE data. Nevertheless, it still makes sense to compare the modified OMI data to the tropospheric NO₂ VCDs extracted from the CHIMERE data, because the modified OMI data only depend on the relative shape of the simulated NO₂ profile, but not on the absolute value of the tropospheric NO₂ VCD.

5.2 Influence of horizontal rotations of the model data on the comparison with OMI

As for the car-MAX-DOAS data, we investigated the effects of rotations of the CHIMERE results around the centre of Paris on the comparison with the OMI data. Two examples are shown in Figs. 15 and 16. On 28 July 2009 (Fig. 15) the emission plume extended in north-east direction. Good spa-
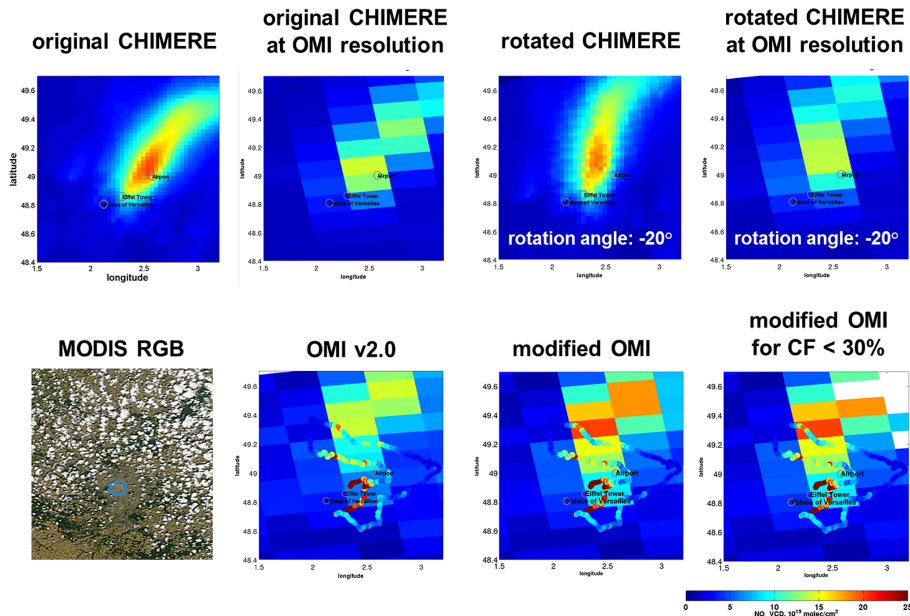
Figure 15. Comparison of different versions of OMI and CHIMERE data for 28 July 2009. Also shown are a MODIS RGB image and the car-MAX-DOAS results of that day.
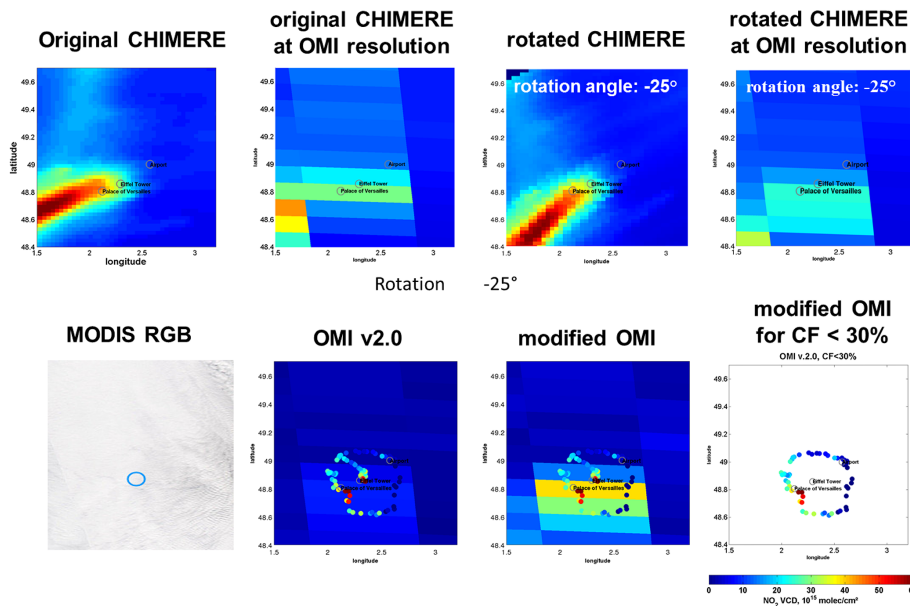

Figure 16. Comparison of different versions of OMI and CHIMERE data for 8 February 2010. Also shown are a MODIS RGB image and the car-MAX-DOAS results of that day.

tial agreement between the model simulations (re-sampled to OMI ground pixel extent) and satellite observations is found after the model data is rotated by $-20°$. On that day the simulated tropospheric NO$_2$ VCDs are systematically underestimated compared to OMI data, especially far away from the city centre (of course, in principle, also the OMI data might have a systematic offset). The differences between model simulations and satellite observations become even larger for

the modified OMI product because for observations of the most polluted areas the replacement of the TM-4 profile by the CHIMERE profile has the strongest effect.

In Fig. 16 results for 8 February 2010 are shown. Although the CF is $> 30\%$ for all OMI measurements on that day, we chose this example to illustrate that even under such unfavourable conditions the satellite observations can yield useful information on the location of the emission plume. Like
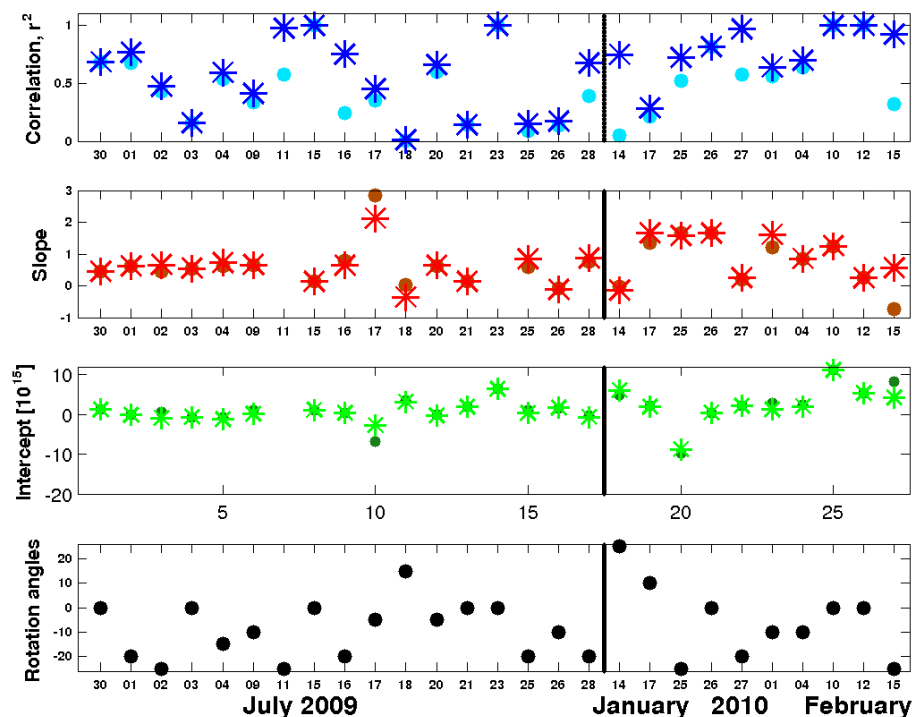
Figure 17. Results of the spatial correlation analyses between CHIMERE and OMI (v2.0 for CF < 30 %) for individual days (dots: results for original CHIMERE data; stars: results for rotated CHIMERE data). **(a)** Correlation coefficients; **(b)** slopes of the regression lines; **(c)** y axis intercepts; **(d)** optimum rotation angles.

for the previous example, good agreement between both data sets is found after the CHIMERE data is rotated by −25°. And also the model data are again systematically smaller than the satellite observations. In spite of the strong influence of clouds on the satellite observation on 8 February 2010, it is interesting to note that the OMI data show enhanced tropospheric NO$_2$ VCDs at similar locations as the model.

Note that similar comparisons between the three data sets for all days of both car-MAX-DOAS campaigns are presented in the Supplement (Fig. S4). Here it should again be noted that for the modified OMI data (see Sect. 5.1) not the original but the rotated CHIMERE profiles were applied to the OMI retrieval. This is an important detail, as the NO$_2$ profiles vary strongly depending on whether they are inside or outside the emission plume.

In Fig. 17 the results of spatial correlation analyses between CHIMERE and OMI for all days with coincident data are shown. Like for the comparison with the car-MAX-DOAS measurements, for most days the rotation of the CHIMERE data leads to an improvement of the correlation coefficients (as has to be expected). However, the improvement of the correlation coefficient is smaller than for the comparison with the car-MAX-DOAS measurements. Also, for the slopes and y axis intercepts, only small changes are found. Both findings indicate that the determination of the rotation is less well constrained by the OMI observations

compared to the car-MAX-DOAS measurements. This can be explained both by the much coarser resolution of the OMI data and the frequent gaps due to clouds. Since the spatial resolution of the CHIMERE data is much finer than the OMI resolution, the shape of the OMI ground pixels has no significant effect on the determination of the rotation angles, as CHIMERE data is re-sampled to the OMI pixel extent.

Figure 18 presents the daily averages and maxima for both data sets for effective CF < 30 %. Like for the comparison between car-MAX-DOAS and CHIMERE, the day to day variability is well represented in both data sets. The average ratios of daily maximum and average values are summarised in Table 3. For the ratios of the averages the modification of the OMI data using the CHIMERE profiles has a small effect. The ratio between CHIMERE and OMI data is about 0.76 in summer and 1.00 in winter. Concerning the maxima, the effect of the modification of the OMI data using the CHIMERE profiles is stronger: the ratios between CHIMERE and OMI data decrease from 0.83 to 0.68 in summer and from 0.85 to 0.80 in winter.

Figure 19 presents the correlation results between CHIMERE and OMI for all individual data pairs. In addition to the original OMI (v2.0) and CHIMERE data, results for the rotated CHIMERE data and the modified OMI data are also shown. Again an orthogonal linear regression is performed, where the uncertainties of the CHIMERE data are

Table 3. Ratios of daily average and maximum values (CHIMERE/OMI) as well as slopes and correlation coefficients of the regression analyses for OMI observations with effective CF below 0.3.

Quantity	Ratio CHIMERE/OMI (v2.0)		Ratio CHIMERE/modified OMI	
	Summer	Winter	Summer	Winter
Ratio of averages	0.74	0.99	0.78	1.00
Ratio of maxima	0.83	0.85	0.68	0.80
Slope (r^2)	0.52 ($r^2 = 0.46$)	1.16 ($r^2 = 0.35$)	0.52 ($r^2 = 0.71$)	0.90 ($r^2 = 0.50$)
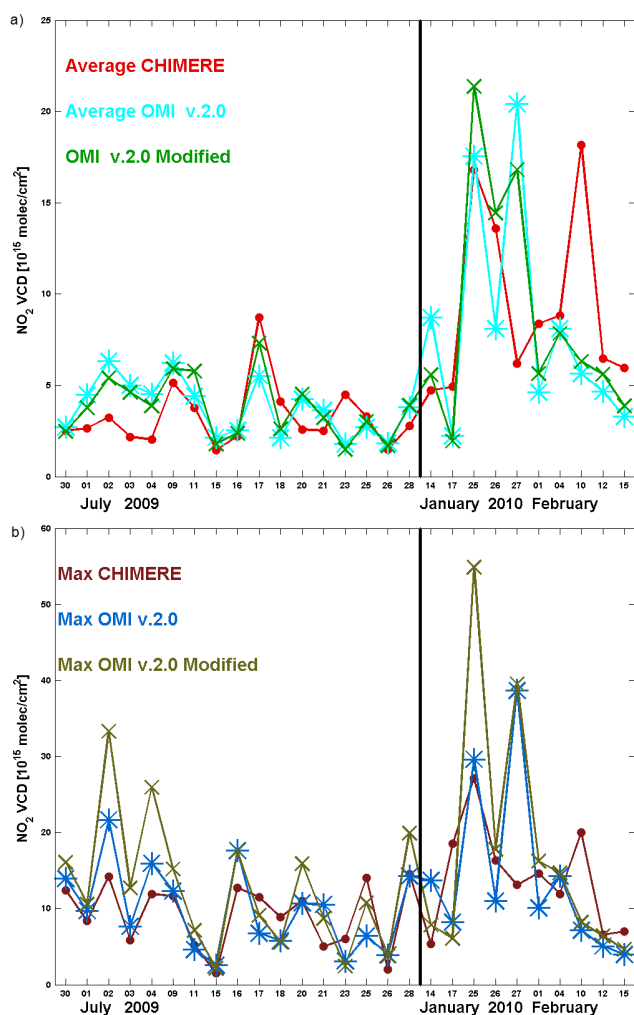
Figure 18. Comparison of the daily average **(a)** and maximum **(b)** tropospheric NO$_2$ VCDs for original and modified OMI observations (CF below 30 %) and coincident CHIMERE data.

described by a constant (2×10^{15} molec cm^{-2}) and a linear term (20 %). For OMI the individual errors are taken from the DOMINO data product (Boersma et al., 2011).

After each modification step the correlations between both data sets improve (r^2 increases from 0.31 to 0.71 in summer and from 0.24 to 0.50 in winter). In contrast, the slopes of the regression lines hardly changes (in winter they even decrease). For the comparison between the rotated CHIMERE and the modified OMI data, the slopes are 0.52 and 0.96, respectively (but for winter the slope has to interpreted with care, because of the rather poor correlation).

5.3 Quantitative interpretation of the comparison results

We quantify the agreement of the tropospheric NO$_2$ background VCDs based on the ratios of the daily average values (Fig. 18a). For winter, the ratios both for the original and the modified OMI data are close to unity (see Table 3), indicating good agreement between both data sets. In contrast, for summer the ratios are much lower (0.74 and 0.76 for the original and modified OMI data, respectively), indicating that CHIMERE systematically underestimates the OMI measurements.

The agreement of the tropospheric NO$_2$ VCDs in the Paris plume is quantified by the ratios of the daily maxima (Fig. 18b) and slopes of the regression lines of the individual data pairs (Fig. 19). For the original OMI data, the ratios and slopes are between 0.52 and 0.83 and between 0.85 and 1.16 for summer and winter, respectively. Overall, these results indicate a systematic underestimation of the OMI data by CHIMERE (the slope of 1.16 is probably not very meaningful because of the rather low correlation coefficient).

If the modified OMI data are considered, the ratios and slopes become even smaller: they are between 0.52 and 0.68 and 0.80 and 0.90 in summer and winter, respectively. This finding reflects the fact that the use of the CHIMERE profiles causes an increase of the OMI results.

6 Comparison between OMI and car-MAX-DOAS

In this section we first directly compare car-MAX-DOAS to OMI observations. Then we use the CHIMERE model as a transfer tool to correct for the differences in the spatial coverage. For the comparison between car-MAX-DOAS and OMI data we averaged all MAX-DOAS measurements within each OMI ground pixel with effective CF below 0.3, for days where large circles around Paris are sampled. Like for the comparison between CHIMERE and car-MAX-DOAS data
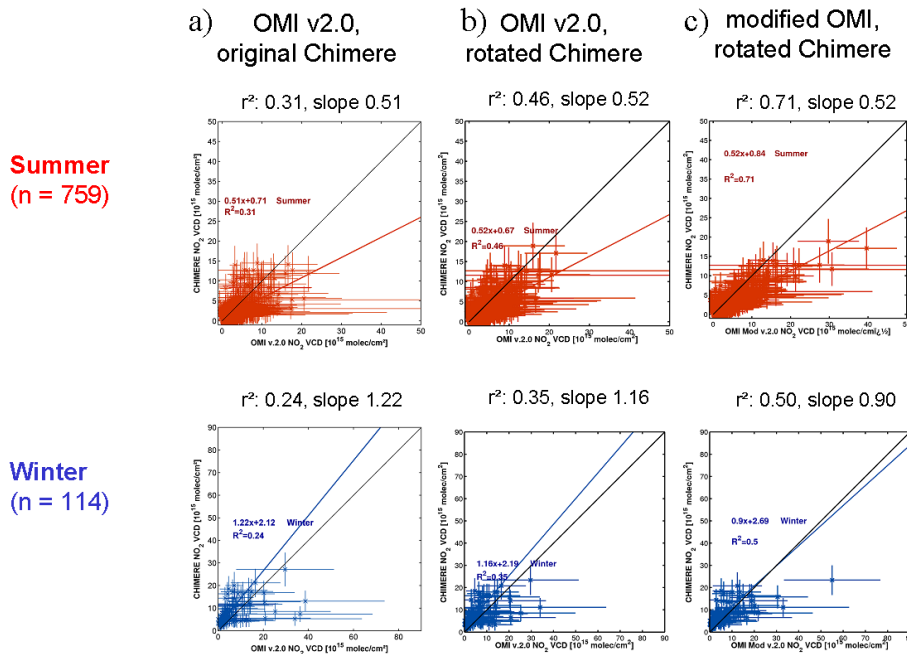
Figure 19. Correlation analyses between CHIMERE and OMI observations (for CF < 30 %) for **(a)** the original data sets, **(b)** rotated CHIMERE data, and **(c)** rotated CHIMERE data and modified OMI data.
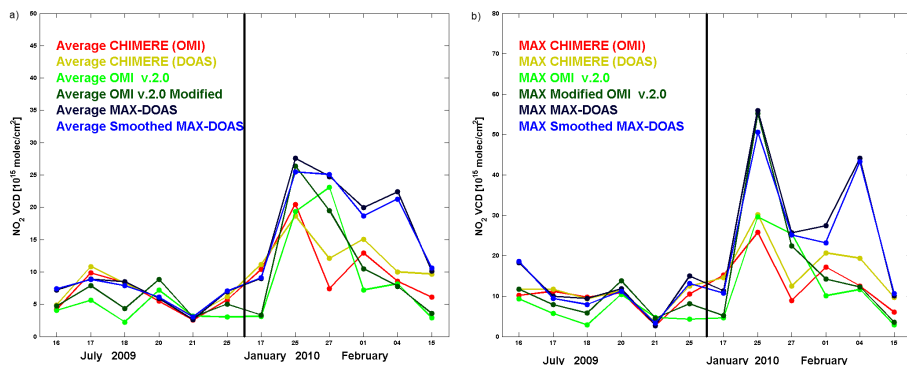

Figure 20. Comparison of the daily average **(a)** and maximum **(b)** tropospheric NO$_2$ VCDs for coincident data of all three data sets (car-MAX-DOAS measurements along large circles and OMI observations for CF < 30 %; rotated CHIMERE data).

(Sect. 4), the choice for large circles was made because for these observations the rotation of the CHIMERE data can be more accurately determined. The rotation angle was determined from the comparison to the car-MAX-DOAS data (see Sect. 4). The (rotated) CHIMERE profiles were used for the modification of the OMI data.

In Fig. 20 the averages of the daily maximum and average values of the different data sets are compared. Overall, the day to day variability of the tropospheric NO$_2$ VCDs is well captured by the three data sets. Here it should be noted that in Fig. 20 two versions of the CHIMERE data are used: CHIMERE (OMI) indicates CHIMERE results averaged over the entire OMI ground pixels, whereas CHIMERE (DOAS) indicates CHIMERE results averaged for the loca-

tions of the coincident car-MAX-DOAS observations. Especially for the maximum values, the specific sampling of the model data has a substantial effect: CHIMERE data sampled at the locations of the car-MAX-DOAS observations are systematically larger than the CHIMERE data sampled over the entire OMI ground pixels, indicating the effect of spatial gradients within the satellite ground pixels.

In Table 4 the average ratios of the daily maximum and average values are shown. In summer, similar ratios for the averages and maxima (about 0.90) are derived for the original and smoothed car-MAX-DOAS data. If, however, the car-MAX-DOAS data are scaled to full OMI pixels (based on CHIMERE spatial patterns), the ratios between OMI and car-MAX-DOAS data becomes close to unity. The correction for

Table 4. Ratios of daily average and maximum values (modified OMI/car-MAX-DOAS) as well as slopes and correlation coefficients of the regression analyses for measurements at large circles and OMI effective CF below 0.3. For the correction of the car-MAX-DOAS observations see text.

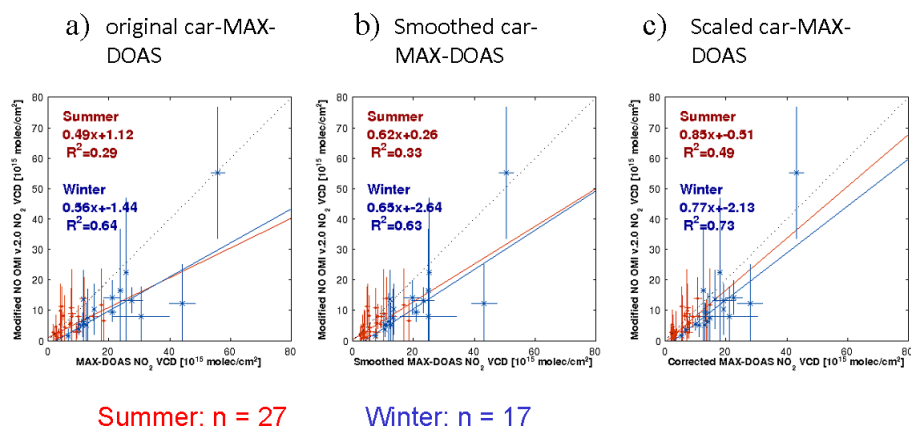| Quantity	Modified OMI/original car-MAX-DOAS		Modified OMI/scaled car-MAX-DOAS	
	Summer	Winter	Summer	Winter
Ratio of averages	0.90	0.56	0.97	0.72
Ratio of maxima	0.91	0.58	1.00	0.82
Slope (r^2)	0.48 ($r^2 = 0.29$)	0.56 ($r^2 = 0.64$)	0.85 ($r^2 = 0.49$)	0.77 ($r^2 = 0.73$)

Figure 21. Correlation analyses between OMI observations (modified version for CF $< 30\%$) and different versions of car-MAX-DOAS observations (along large circles). **(a)** Original car-MAX-DOAS; **(b)** smoothed car-MAX-DOAS; **(c)** car-MAX-DOAS corrected for spatial gradients within the satellite ground pixels (see text).

the effect of spatial gradients is performed by multiplying the car-MAX-DOAS data by the average ratio CHIMERE (OMI)/CHIMERE (DOAS), which is ∼ 0.90.

For winter, again similar ratios for the averages and maxima are found for the original and smoothed car-MAX-DOAS data, but now they are much lower (around 0.60). After correction for the effect of spatial gradients within the satellite ground pixels, the ratios increase from 0.72 to 0.82, but still are systematically below unity, indicating that the OMI results underestimate the car-MAX-DOAS data.

The results of the correlation analyses for individual measurements are shown in Fig. 21. Again an orthogonal linear regression is performed, where the uncertainties of the car-MAX-DOAS data are described by the standard deviation of the individual observations divided by the number of observations inside the OMI pixels. For OMI the individual errors are taken from the DOMINO data product (Boersma et al., 2011).

The different sub-plots show results for different versions of the car-MAX-DOAS data: original car-MAX-DOAS data (Fig. 21a), smoothed car-MAX-DOAS data (Fig. 21b) and scaled car-MAX-DOAS (Fig. 21c). Here the car-MAX-DOAS data are again scaled to the full OMI pixels, but now the correction is applied for individual car-MAX-

DOAS measurements using the respective ratios CHIMERE (OMI)/CHIMERE (DOAS). The correction of the car-MAX-DOAS data leads to a much better agreement between both data sets: the correlation coefficients r^2 increase from 0.29 to 0.49 in summer, and from 0.64 to 0.73 in winter. The slopes increase from 0.49 to 0.85 in summer, and from 0.56 to 0.77 in winter. It should, however, be noted that the slopes of the regression lines are still smaller than unity, indicating that OMI underestimates the tropospheric NO$_2$ VCD in the emission plume of Paris.

6.1 Quantitative interpretation of the comparison results

We quantify the agreement of the tropospheric NO$_2$ background VCDs based on the ratios of the daily average values (Fig. 20). For summer, the ratios are 0.90 and 0.97 for the original and scaled car-MAX-DOAS data, respectively, indicating a slight underestimation of the car-MAX-DOAS data by OMI. For winter, the ratios are much smaller: they are 0.56 and 0.72 for the original and scaled car-MAX-DOAS data, respectively, indicating a strong underestimation of the car-MAX-DOAS data by OMI.

Table 5. Summary of the quantitative comparisons between the three data sets for different data selections. The background results are derived from the ratios of the daily averages. The results for the emission plumes are derived from the ratios of the daily maximum values and the correlation analyses of the individual observations. Note that for both data selections the results for the comparison between OMI and car-MAX-DOAS are the same, because CHIMERE data are available for all days.

(a) Coincidences of all three data sets						
Case	CHIMERE[a]/DOAS[b]		OMI[c]/DOAS[b]		CHIMERE[a]/OMI[c]	
	Summer	Winter	Summer	Winter	Summer	Winter
Background	1.01	0.87	0.97	0.72	0.78	1.00
Emission plume	0.70–0.94	0.64–0.75	0.73–0.82	0.85–1.00	0.52–0.68	0.80–0.90
(b) Coincidences of two data sets						
Case	CHIMERE[a]/DOAS[b]		OMI[c]/DOAS[b]		CHIMERE[a]/OMI[c]	
	Summer	Winter	Summer	Winter	Summer	Winter
Background	0.93	0.69	0.97	0.72	0.98	0.92
Emission plume	0.78–0.96	0.45–0.68	0.73–0.82	0.85–1.00	0.97–1.04	0.81–0.93

[a] Rotated CHIMERE; [b] scaled car-MAX-DOAS; [c] modified OMI.

The agreement of the tropospheric NO$_2$ VCDs of the emission plume is quantified by the ratios of the daily maxima (Fig. 20) and slopes of the regression lines of the individual data pairs (Fig. 21). For the original car-MAX-DOAS data, the ratios and slopes are between 0.48 and 0.91 and between 0.56 and 0.58 for summer and winter, respectively, indicating a substantial underestimation of the car-MAX-DOAS data by OMI. If the scaled car-MAX-DOAS data are considered, the ratios and slopes increase: they are between 0.85 and 1.00 and between 0.77 and 0.82 in summer and winter, respectively, indicating a weaker, but still systematic underestimation of the car-MAX-DOAS data by OMI.

We also compared the original OMI data (v2.0) to the car-MAX-DOAS observations (see Fig. S3). Like for the modified OMI data, better agreement is found after applying the correction for the spatial gradients inside the OMI ground pixels to the car-MAX-DOAS data. However, the correlation coefficients and slopes are much smaller than for the comparison with the modified OMI data, indicating the importance of using appropriate NO$_2$ profiles for the processing of the satellite data close to strong emission sources.

6.2 Comparison with the results of the bilateral comparisons OMI versus CHIMERE and car-MAX-DOAS versus CHIMERE

The data selection in this section is quite different compared to the selections for the bilateral comparisons presented in Sect. 4 and 5. Especially for the comparison between OMI and CHIMERE much larger areas are covered in Sect. 5. Thus it is interesting to see how the different data selections affect the comparison results. In Table 5 the respective ratios of daily averages and maxima as well as the results of the regression analyses are compared for the different data selections.

For the comparison between CHIMERE and car-MAX-DOAS slightly higher ratios are found if only coincident CHIMERE and car-MAX-DOAS data are compared (the additional constraint of coincident OMI observations mainly excludes cloudy situations from the comparison, because only OMI observations with effective CF below 0.3 are considered). This finding probably indicates that car-MAX-DOAS observations under mostly overcast conditions slightly underestimate the true tropospheric NO$_2$ VCD, because a small fraction of the tropospheric NO$_2$ VCDs might be inside the cloud layer.

For the comparison between CHIMERE and OMI similar ratios are found for winter, but in summer CHIMERE underestimates the OMI observations more than for the comparison presented in Sect. 5. This discrepancy is probably related to the fact that the observations selected in Sect. 5 cover a much larger area around Paris and indicates that the underestimation of the OMI data by CHIMERE increases with increasing distance from the emission source. One possible explanation for this finding is that the underestimation of the NO$_x$ lifetime in the CHIMERE model (potentially due to too high OH levels). Another possibility could be that the NO$_2$ profiles used in the OMI analysis might be more appropriate close to the emission sources.

7 Summary and outlook

In this study we compared extensive data sets of tropospheric NO$_2$ VCDs obtained from car-MAX-DOAS observations in the Paris metropolitan area with coincident satellite measurements from OMI and results from the regional model CHIMERE. The car-MAX-DOAS measurements were carried out on 25 days in summer 2009 and 29 days in winter 2010 within the European research project MEGAPOLI

(Mahura and Baklanov, 2011). On most of these days car-MAX-DOAS measurements were made along large circles (diameter $\sim$ 35 km) around Paris. The duration of individual car-MAX-DOAS measurements was about 1 min corresponding to about 1 km. The car-MAX-DOAS measurements were primarily made to determine the entire NO$_x$ emissions from Paris (see e.g. Shaiganfar et al., 2011). The derived NO$_x$ emissions will be published in a separate paper (Shaiganfar et al., 2015). In this study we focus on the direct comparison of the car-MAX-DOAS results with the two other data sets.

All three data sets all have their specific strengths and weaknesses, especially with respect to their spatiotemporal resolution and coverage as well as their uncertainties. Car-MAX-DOAS have rather small uncertainties and high spatial resolution, but provide only small spatiotemporal coverage. Satellite observations cover the area of interest on a daily basis, but with a rather coarse spatial resolution and relatively large uncertainties. The influence of clouds on the satellite results is strong, and usually only measurements with low effective CF provide meaningful information on the tropospheric NO$_2$ VCD (here we use measurements with effective CF below 30 %).

First we directly compare the original versions of the three data sets. Here, rather large systematic differences and low correlations are found. In particular the enhanced NO$_2$ VCDs inside the emission plume from Paris measured by car-MAX-DOAS are largely underestimated by the satellite observations and model results. In a second attempt, we compare the three data sets after they were modified by making synergistic use of the specific advantages of the different data sets:

– CHIMERE model results were rotated around the centre of Paris until best spatial agreement with car-MAX-DOAS or satellite measurements was obtained. The observation of a "tilt" between the spatial patterns of CHIMERE and MAXDOAS are probably related to a mismatch in wind direction in the MM5 meteorological model. A spatial misplacement of emissions in the Paris region, in particular as a function of the distance from Paris centre, is also a possible error source, as has been shown by comparing NO$_x$ emission fields in and around the Paris agglomeration from different emission inventories (Petetin et al., 2014).

– Car-MAX-DOAS measurements were spatially smoothed until best match with the model data was achieved. The resulting smoothing Kernels of about 6–8 km suggest an effective resolution of CHIMERE of this order.

– OMI data were corrected by using the vertical NO$_2$ concentration profiles from the regional CHIMERE model.

– The effect of spatial gradients within the satellite ground pixels on the comparison between car-MAX-DOAS and OMI observations was accounted for and partially corrected using the CHIMERE model data.

The last two points underline the need for a regional model in order to compare MAX-DOAS with satellite measurements in a meaningful way.

Using these modified data sets, the correlation of individual data pairs largely improved. Also, much better quantitative agreement between the data sets was found. However, still the satellite observations and the CHIMERE model results systematically underestimate the car-MAX-DOAS observations inside the emission plume from Paris, although the underestimation is much less compared to the original data sets. For the tropospheric NO$_2$ VCDs outside the emission plume, a much better agreement is found.

From these results we conclude that close to strong emission sources, the applied improvements of the observational and simulation data sets are essential for a meaningful quantitative comparison of the tropospheric NO$_2$ VCDs; for example, in the measurements in the Paris metropolitan area, about 10–40 % of the observed differences can be attributed to the effects of spatial gradients (see also Chen et al., 2009; Ma et al., 2013; Lin et al., 2014). By not properly considering these effects, wrong conclusions on the accuracy of the considered data sets of the same order may be drawn. Information on the spatial gradients within the satellite ground pixels may be obtained e.g. by simultaneously using multiple car-MAX-DOAS measurements, or by combining (car-) MAX-DOAS measurements with results from a regional model. Similar changes of the absolute values may occur if inappropriate vertical profiles are used in the satellite data analysis.

One additional interesting finding of our study is that in summer the underestimation of the OMI observations by the CHIMERE model increases with increasing distance from the emission source. This finding could indicate a too low atmospheric NO$_x$ lifetime in the model simulations.

We suggest that future studies should use more sophisticated methods for the extraction of the tropospheric NO$_2$ VCD from car-MAX-DOAS measurements than the geometric approximation. In particular, radiative transfer simulations should be applied taking into account the dependence from SZA and relative azimuth angle. Improved car MAX-DOAS results will especially be important for the validation of new satellite measurements with largely improved spatial resolution (like the future satellite missions Sentinel-5 precursor, Sentinel 4 and 5, see Ingmann et al., 2012; Veefkind et al., 2012).

The Supplement related to this article is available online at doi:10.5194/amt-8-2827-2015-supplement.

Edited by: M. Van Roozendael

References

Airparif Report: La qualité de l'air en 2013 à Paris, available at: http://www.airparif.asso.fr/_pdf/publications/Rbilan75_2013.pdf (last access: 2 March 2015), 2014.

Atkinson, R.: Atmospheric chemistry of VOCs and NO$_x$, Atmos. Environ., 34, 2063–2101, doi:10.1016/S1352-2310(99)00460-4, 2000.

Beekmann, M. and Vautard, R.: A modelling study of photochemical regimes over Europe: robustness and variability, Atmos. Chem. Phys., 10, 10067–10084, doi:10.5194/acp-10-10067-2010, 2010.

Beirle, S., Platt, U., Wenig, M., and Wagner, T.: Weekly cycle of NO$_2$ by GOME measurements: a signature of anthropogenic sources, Atmos. Chem. Phys., 3, 2225–2232, doi:10.5194/acp-3-2225-2003, 2003.

Beirle, S., Boersma, K. F., Platt, U., Lawrence, M. G., and Wagner, T.: Megacity emissions and lifetimes of nitrogen oxides probes from space, Science, 333, 1737–1739, doi:10.1126/science.1207824, 2011.

Boersma, K. F., Bucsela, E. J., Brinksma, E. J., and Gleason, J. F.: NO$_2$, in: OMI Algorithm Theoretical Basis Document, vol. 4, OMI Trace Gas Algorithms, ATB-OMI-04, Version 2.0, edited by: Chance, K., NASA Distrib. Active Archive Cent., Greenbelt, Md., 13–36, 2002.

Boersma, K. F., Eskes, H. J., and Brinksma, E. J.: Error analysis for tropospheric NO$_2$ retrieval from space, J. Geophys. Res., 109, D04311, doi:10.1029/2003JD003962, 2004.

Boersma, K. F., Eskes, H. J., Veefkind, J. P., Brinksma, E. J., van der A, R. J., Sneep, M., van den Oord, G. H. J., Levelt, P. F., Stammes, P., Gleason, J. F., and Bucsela, E. J.: Near-real time retrieval of tropospheric NO$_2$ from OMI, Atmos. Chem. Phys., 7, 2103–2118, doi:10.5194/acp-7-2103-2007, 2007.

Boersma, K. F., Eskes, H. J., Dirksen, R. J., van der A, R. J., Veefkind, J. P., Stammes, P., Huijnen, V., Kleipool, Q. L., Sneep, M., Claas, J., Leitão, J., Richter, A., Zhou, Y., and Brunner, D.: An improved tropospheric NO$_2$ column retrieval algorithm for the Ozone Monitoring Instrument, Atmos. Meas. Tech., 4, 1905–1928, doi:10.5194/amt-4-1905-2011, 2011.

Bogumil, K., Orphal, J., Homann, T., Voigt, S., Spietz, P., Fleischmann, O. C., Vogel, A., Hartmann, M., Bovensmann, H., Frerik, J., and Burrows, J. P.: Measurements of Molecular Absorption Spectra with the SCIAMACHY Pre-Flight Model: Instrument Characterization and Reference Data for Atmospheric Remote-Sensing in the 230–2380 nm Region, J. Photochem. Photobiol. A., 157, 167–184, 2003.

Boynard, A., Beekmann, M., Foret, G., Ung, A., Szopa, S., Schmechtig, C., and Coman, A.: Assessment of regional ozone model uncertainty with an explicit error representation, Atmos. Environ., 45, 763–781, 2011.

Brewer, A. W., McElroy, C. T., and Kerr, J. B., Nitrogen dioxide concentrations in the atmosphere, Nature, 246, 129–133, 1973.

Brinksma, E. J., Pinardi, G., Volten, H., Braak, R., Richter, A., Schönhardt, A., Van Roozendael, M., Fayt, C., Hermans, C., Dirksen, R. J., Vlemmix, T., Berkhout, A. J. C., Swart, D. P. J., Ötjen, H., Wittrock, F., Wagner, T., Ibrahim, O. W., de Leeuw, G., Moerman, M., Curier, R. L., Celarier, E. A., Knap, W. H., Veefkind, J. P., Eskes, H. J., Allaart, M., Rothe, R., Piters, A. J. M., and Levelt, P. F.: The 2005 and 2006 DANDELIONS NO$_2$ and Aerosol Validation Campaigns, J. Geophys. Res., 113, D16S46, doi:10.1029/2007JD008808, 2008.

Cantrell, C. A.: Technical Note: Review of methods for linear least-squares fitting of data and application to atmospheric chemistry problems, Atmos. Chem. Phys., 8, 5477–5487, doi:10.5194/acp-8-5477-2008, 2008.

Chen, D., Zhou, B., Beirle, S., Chen, L. M., and Wagner, T.: Tropospheric NO$_2$ column densities deduced from zenith-sky DOAS measurements in Shanghai, China, and their application to satellite validation, Atmos. Chem. Phys., 9, 3641–3662, doi:10.5194/acp-9-3641-2009, 2009.

Deguillaume L., Beekmann, M., and Menut, L.: Bayesian Monte Carlo analysis applied to regional scale inverse emission modelling for reactive trace gases, J. Geophys. Res., 112, D02307, doi:10.1029/2006JD007518, 2007.

Dieudonné E., Ravetta, F., Pelon, J., Goutail, F., and Pommereau, J.-P.: Linking NO$_2$ surface concentration and integrated content in the urban developed atmospheric boundary layer, Geophys. Res. Lett., 40, 1247–1251, 2013.

Dudhia, J.: A nonhydrostatic version of the Penn State ÄìNCAR Mesoscale Model: validation tests and simulation of an Atlantic cyclone and cold front, Mon. Weather Rev., 121, 1493–1513, 1993.

Folberth, G. A., Hauglustaine, D. A., Lathière, J., and Brocheton, F.: Interactive chemistry in the Laboratoire de Météorologie Dynamique general circulation model: model description and impact analysis of biogenic hydrocarbons on tropospheric chemistry, Atmos. Chem. Phys., 6, 2273–2319, doi:10.5194/acp-6-2273-2006, 2006.

Frieß, F., Monks, P. S., Remedios, J. J., Rozanov, A., Sinreich, R., Wagner, T., and Platt, U.: MAX-DOAS O4 measurements: a new technique to derive information on atmospheric aerosols, (II) modelling studies, J. Geophys. Res., 111, D14203, doi:10.1029/2005JD006618, 2006.

Guenther, A., Karl, T., Harley, P., Wiedinmyer, C., Palmer, P. I., and Geron, C.: Estimates of global terrestrial isoprene emissions using MEGAN (Model of Emissions of Gases and Aerosols from Nature), Atmos. Chem. Phys., 6, 3181–3210, doi:10.5194/acp-6-3181-2006, 2006.

Haeffelin, M., Barthès, L., Bock, O., Boitel, C., Bony, S., Bouniol, D., Chepfer, H., Chiriaco, M., Cuesta, J., Delanoë, J., Drobinski, P., Dufresne, J.-L., Flamant, C., Grall, M., Hodzic, A., Hourdin, F., Lapouge, F., Lemaître, Y., Mathieu, A., Morille, Y., Naud, C., Noël, V., O'Hirok, W., Pelon, J., Pietras, C., Protat, A., Romand, B., Scialom, G., and Vautard, R.: SIRTA, a ground-based atmospheric observatory for cloud and aerosol research, Ann. Geophys., 23, 253–275, doi:10.5194/angeo-23-253-2005, 2005.

Hains, J. C., Boersma, F. K., Kroon, M., Dirksen, R. J., Cohen, R. C., Perring, A. E., Bucsela, E., Volten, H., Swart, D. P. J., Richter, A., Wittrock, F., Schoenhardt, A., Wagner, T., Ibrahim, O. W., van Roozendael, M., Pinardi, G., Gleason, J. F., Veefkind, J. P., and Levelt, P.: Testing and improving OMI DOMINO tropospheric NO$_2$ using observations from the DANDELIONS and INTEX-B validation campaigns, J. Geophys. Res., 115, D05301, doi:10.1029/2009JD012399, 2010.

Hansen, M. C., Defries, R. S., Townshend, J. R. G., and Sohlberg, R.: Global land cover classification at 1 km spatial resolution using a classification tree approach, Int. J. Remote Sens., 21, 1331–1364, 2000.

Hauglustaine, D. A., Hourdin, F., Jourdain, L., Filiberti, M.-A., Walters, S., Lamarque, J.-F., and Holland, E. A.: Interactive chemistry in the Laboratoire de Meteorologie Dynamique general circulation model: description and background tropospheric chemistry evaluation. J. Geophys. Res., 109, D04314, doi:10.1029/2003JD003957, 2004.

Hermans, C., Vandaele, A. C., Carleer, M., Fally, S., Colin, R., Jenouvrier, A., and Mérienne, M. F.: Absorption cross-sections of atmospheric constituents: NO$_2$, O$_2$, and H$_2$O, Environ. Sci. Poll. Res., 6, 151–158, 1999.

Hönninger G. and Platt, U.: Observations of BrO and its vertical distribution during surface ozone depletion at Alert, Atmos. Environ., 36, 2481–2490, 2002.

Honoré, C., Rouil, L., Vautard, R., Beekmann, M., Bessagnet, B., Dufour, A., Elichegaray, C., Flaud, J.-M., Malherbe, L., Meleux, F., Menut, L., Martin, D., Peuch, A., Peuch, V. H., and Poisson, N.: Predictability of European air quality: the assessment of three years of operational forecasts and analyses by the PREV'AIR system, J. Geophys. Res., 113, D04301, doi:10.1029/2007JD008761, 2008.

Ibrahim, O., Shaiganfar, R., Sinreich, R., Stein, T., Platt, U., and Wagner, T.: Car MAX-DOAS measurements around entire cities: quantification of NO$_x$ emissions from the cities of Mannheim and Ludwigshafen (Germany), Atmos. Meas. Tech., 3, 709–721, doi:10.5194/amt-3-709-2010, 2010.

Ingmann, P., Veihelmann, B., Langen, J., Lamarre, D., Stark, H., and Courrèges-Lacoste, G. B.: Requirements for the GMES Atmosphere Service and ESA's implementation concept: sentinels-4/-5 and -5p, Remote Sens. Environ., 120, 58–69, doi:10.1016/j.rse.2012.01.023, 2012.

Irie, H., Boersma, K. F., Kanaya, Y., Takashima, H., Pan, X., and Wang, Z. F.: Quantitative bias estimates for tropospheric NO$_2$ columns retrieved from SCIAMACHY, OMI, and GOME-2 using a common standard for East Asia, Atmos. Meas. Tech., 5, 2403–2411, doi:10.5194/amt-5-2403-2012, 2012.

Konovalov, I. B., Beekmann, M., Richter, A., and Burrows, J. P.: Inverse modelling of the spatial distribution of NOx emissions on a continental scale using satellite data, Atmos. Chem. Phys., 6, 1747–1770, doi:10.5194/acp-6-1747-2006, 2006.

Kuenen, J. J. P., Visschedijk, A. J. H., Jozwicka, M., and Denier van der Gon, H. A. C.: TNO-MACC_II emission inventory; a multi-year (2003–2009) consistent high-resolution European emission inventory for air quality modelling, Atmos. Chem. Phys., 14, 10963–10976, doi:10.5194/acp-14-10963-2014, 2014.

Leue, C., Wenig, M., Wagner, T., Platt, U., and Jähne, B.: Quantitative analysis of NO$_x$ emissions from GOME satellite image sequences, J. Geophys. Res., 106, 5493–5505, 2001.

Levelt, P., Van den Oord, G., Dobber, M., Malkki, A., Visser, H., de Vries, J., Stammes, P., Lundell, J., and Saari, H.: The Ozone Monitoring Instrument, IEEE T. Geosci. Remote, 44, 1093–1101, doi:10.1109/TGRS.2006.872333, 2006.

Lin, J.-T., Martin, R. V., Boersma, K. F., Sneep, M., Stammes, P., Spurr, R., Wang, P., Van Roozendael, M., Clémer, K., and Irie, H.: Retrieving tropospheric nitrogen dioxide from the Ozone Monitoring Instrument: effects of aerosols, surface reflectance anisotropy, and vertical profile of nitrogen dioxide, Atmos. Chem. Phys., 14, 1441–1461, doi:10.5194/acp-14-1441-2014, 2014.

Ma, J. Z., Beirle, S., Jin, J. L., Shaiganfar, R., Yan, P., and Wagner, T.: Tropospheric NO$_2$ vertical column densities over Beijing: results of the first three years of ground-based MAX-DOAS measurements (2008–2011) and satellite validation, Atmos. Chem. Phys., 13, 1547–1567, doi:10.5194/acp-13-1547-2013, 2013.

Mahura, A. and Baklanov, A.: Megapoli Newsletters, Megapoli Project, ISBN: 978-87-92731-27-2, available at: http://megapoli.dmi.dk/nlet/MEGAPOLI_NewsLet01.pdf (last access: 1 December 2011), MEGAPOLI document (MEGAPOLI-01-MNL-11-09), 2011.

Martin, R. V., Chance, K., Daniel, J. J., Kurosu, T. P., Spurr, R. J. D., Bucsela, E., Gleason, J. F., Palmer, P. I., Bey, I., Fiore, A. M., Li, Q., Yantosca, R. M., and Koelemeijer, R. B. A.: An improved retrieval of tropospheric nitrogen dioxide from GOME, J. Geophys. Res., 107, 4437, doi:10.1029/2001JD001027, 2002.

Martin, R. V., Jacob, D. J., Chance, K., Kurosu, T. P., Palmer, P. I., and Evans, M. J.: Global inventory of nitrogen oxide emissions constrained by space-based observations of NO$_2$ columns, J. Geophys. Res., 108, 4537, doi:10.1029/2003JD003453, 2003.

Menut, L., Bessagnet, B., Khvorostyanov, D., Beekmann, M., Blond, N., Colette, A., Coll, I., Curci, G., Foret, G., Hodzic, A., Mailler, S., Meleux, F., Monge, J.-L., Pison, I., Siour, G., Turquety, S., Valari, M., Vautard, R., and Vivanco, M. G.: CHIMERE 2013: a model for regional atmospheric composition modelling, Geosci. Model Dev., 6, 981–1028, doi:10.5194/gmd-6-981-2013, 2013.

Noxon, J. F.: Nitrogen dioxide in the stratosphere and troposphere measured by ground-based absorption spectroscopy, Science, 189, 547–549, 1975.

Petetin, H., Beekmann, M., Colomb, A., Denier van der Gon, H. A. C., Dupont, J.-C., Honoré, C., Michoud, V., Morille, Y., Perrussel, O., Schwarzenboeck, A., Sciare, J., Wiedensohler, A., and Zhang, Q. J.: Evaluating BC and NO$_x$ emission inventories for the Paris region from MEGAPOLI aircraft measurements, Atmos. Chem. Phys. Discuss., 14, 29237–29304, doi:10.5194/acpd-14-29237-2014, 2014.

Pielke Sr, R. A.: Mesoscale meteorological modeling, Vol. 98, Academic press is an imprint of Elsevier, Waltham, MA, USA, p. 89, 2013.

Platt, U. and Stutz, J.: Differential Absorption Spectroscopy, Springer, Berlin, Heidelberg, 135–174, 2008.

Richter, A. and Burrows, J. P.: Tropospheric NO$_2$ from GOME Measurements, Adv. Space Res., 29, 1673–1683, 2002.

Richter, A., Burrows, J. P., Nüß, H., Granier, C., and Niemeier, U.: Increase in tropospheric nitrogen dioxide over China observed from space, Nature, 437, 129–132, doi:10.1038/nature04092, 2005.

Rivera, C., Sosa, G., Wöhrnschimmel, H., de Foy, B., Johansson, M., and Galle, B.: Tula industrial complex (Mexico) emissions of SO$_2$ and NO$_2$ during the MCMA 2006 field campaign using a mobile mini-DOAS system, Atmos. Chem. Phys., 9, 6351–6361, doi:10.5194/acp-9-6351-2009, 2009.

Roscoe, H. K., Johnston, P. V., Van Roozendael, M., Richter, A., Sarkissian, A., Roscoe, J., Preston, K. E., Lambert, J.-C., Hermans, C., Decuyper, W., Dzienus, S., Winterrath, T., Burrows, J., Goutail, F., Pommereau, J.-P., D'Almeida, E., Hottier, J., Coureul, C., Didier, R., Pundt, I., Bartlett, L. M., McElroy, C. T., Kerr, J. E., Elokhov, A., Giovanelli, G., Ravegnani, F., Premuda, M., Kostadinov, I., Erle, F., Wagner, T., Pfeilsticker, K., Kenntner, M., Marquard, L. C., Gil, M., Puentedura, O., Yela, M., Arlander, D. W., Kastad Hoiskar, B. A., Tellefsen, C. W., Karlsen Tornkvist, K., Heese, B., Jones, R. L., Aliwell, S. R., and Freshwater, R. A.: Slant column measurements of O$_3$ and NO$_2$ during the NDSC Intercomparison of Zenith-Sky UV-Visible Spectrometers in June 1996, J. Atmos. Chem., 32, 281–314, 1999.

Rothman, L. S., Jacquemart, D., Barbe, A., Benner, D. C., Birk, M., Brown, L. R., Carleer, M. R., Chackerian Jr., C., Chance, K., Coudert, L. H., Dana, V., Devi, V. M., Flaud, J.-M., Gamache, R. R., Goldman, J.-M., Hartmann, K., Jucks, W., Maki, A. G., Mandin, J.-Y., Massie, S. T., Orphal, J., Perrin, A., Rinsland, C. P., Smith, M. A. H., Tennyson, J., Tolchenov, R. N., Toth, R. A., Vander Auwera, J., Varanasi, P., and Wagner, G.: The HITRAN 2004 molecular spectroscopic database, J. Quant. Spectrosc. Ra., 96 139–204, 2005.

Schmidt, H., Derognat, C., Vautard, R., and Beekmann, M.: A comparison of simulated and observed ozone mixing ratios for the summer of 1998 in western Europe, Atmos. Environ., 35, 6277–6297, 2001.

Seinfeld, J. H. and Pandis, S. N.: Chapter 6.5: The NO$_x$ and NO$_y$ Families, in: Atmospheric Chemistry and Physics: From Air Pollution to Climate Change, John Wiley & Sons, 224–225, 2012.

Shaiganfar, R., Beirle, S., Sharma, M., Chauhan, A., Singh, R. P., and Wagner, T.: Estimation of NO$_x$ emissions from Delhi using Car MAX-DOAS observations and comparison with OMI satellite data, Atmos. Chem. Phys., 11, 10871–10887, doi:10.5194/acp-11-10871-2011, 2011.

Shaiganfar, R., Beirle, S., Petetin, H., Zhang, Q., Beekmann, M., and Wagnet, T.: Estimation of NO$_x$ Emissions from Paris using mobile MAX-DOAS and satellite observations and CHIMERE model, Atmos. Chem. Phys, in preparation, 2015.

Timmermans, R. M. A., Denier van der Gon, H. A. C., Kuenen, J. J. P., Segers, A. J., Honoré, C., Perrussel, O., Builtjes, P. J. H., and Schaap, M.: Quantification of the urban air pollution increment and its dependency on the use of down-scaled and bottom-up city emission inventories, Urban Climate, 6, 46–62, 2013.

Vandaele, A. C., Hermans, C., Simon, P. C., Carleer, M., Colin, R., Fally, S., Mérienne, M.-F., Jenouvrier, A., and Coquart, B.: Measurements of the NO$_2$ Absorption Cross-section from 42000 cm^{-1} to 10 000 cm^{-1} (238–1000 nm) at 220 K and 294 K, J. Quant. Spectrosc. Ra., 59, 171–184, 1997.

Van Roozendael, M., Fayt, C., Post, P., Hermans, C., and Lambert, J.-C.: Retrieval of BrO and NO$_2$ from UV-Visible Observations, in: Sounding the Troposphere From Space: a New Era For Atmospheric Chemistry, edited by: Borell, P., Borrell, P. M., Burrows, J. P., and Platt, U., Springer, Heidelberg, ISBN 3-540-40873-8, 160–162, 2004.

Valari, M. and Menut, L.: Does an increase in air quality models' resolution bring surface ozone concentrations closer to reality?, J. Atmos. Ocean. Tech., 25, 1955–1968, 2008.

Veefkind, J. P., Aben, I., McMullan, K., Förster, H., de Vries, J., Otter, G., Claas, J., Eskes, H. J., de Haan, J. F., Kleipool, Q., van Weele, M., Hasekamp, O., Hoogeveen, R., Landgraf, J., Snel, R., Tol, P., Ingmann, P., Voors, R., Kruizinga, B., Vink, R., Visser, H., and Levelt, P. F.: TROPOMI on the ESA Sentinel-5 Precursor: a GMES mission for global observations of the atmospheric composition for climate, air quality and ozone layer applications, Remote Sens. Environ., 120, 70–83, doi:10.1016/j.rse.2011.09.027, 2012.

Volkamer, R., Spietz, P., Burrows, J. P., and Platt, U.: High-resolution absorption cross-section of Glyoxal in the UV/vis and IR spectral ranges, J. Photoch. Photobio. A, 172, 35–46, doi:10.1016/j.jphotochem.2004.11.011, 2005.

Wagner, T., Beirle, S., and Deutschmann, T.: Three-dimensional simulation of the Ring effect in observations of scattered sun light using Monte Carlo radiative transfer models, Atmos. Meas. Tech., 2, 113–124, doi:10.5194/amt-2-113-2009, 2009.

Wagner, T., Ibrahim, O., Shaiganfar, R., and Platt, U.: Mobile MAX-DOAS observations of tropospheric trace gases, Atmos. Meas. Tech., 3, 129–140, doi:10.5194/amt-3-129-2010, 2010.

Wagner, T., Beirle, S., Brauers, T., Deutschmann, T., Frieß, U., Hak, C., Halla, J. D., Heue, K. P., Junkermann, W., Li, X., Platt, U., and Pundt-Gruber, I.: Inversion of tropospheric profiles of aerosol extinction and HCHO and NO$_2$ mixing ratios from MAX-DOAS observations in Milano during the summer of 2003 and comparison with independent data sets, Atmos. Meas. Tech., 4, 2685–2715, doi:10.5194/amt-4-2685-2011, 2011.

Wittrock, F., Oetjen, H., Richter, A., Fietkau, S., Medeke, T., Rozanov, A., and Burrows, J. P.: MAX-DOAS measurements of atmospheric trace gases in Ny-Ålesund – Radiative transfer studies and their application, Atmos. Chem. Phys., 4, 955–966, doi:10.5194/acp-4-955-2004, 2004.

Zhang, Q. J., Beekmann, M., Drewnick, F., Freutel, F., Schneider, J., Crippa, M., Prevot, A. S. H., Baltensperger, U., Poulain, L., Wiedensohler, A., Sciare, J., Gros, V., Borbon, A., Colomb, A., Michoud, V., Doussin, J.-F., Denier van der Gon, H. A. C., Haeffelin, M., Dupont, J.-C., Siour, G., Petetin, H., Bessagnet, B., Pandis, S. N., Hodzic, A., Sanchez, O., Honoré, C., and Perrussel, O.: Formation of organic aerosol in the Paris region during the MEGAPOLI summer campaign: evaluation of the volatility-basis-set approach within the CHIMERE model, Atmos. Chem. Phys., 13, 5767–5790, doi:10.5194/acp-13-5767-2013, 2013.